Surveys in Geophysics (2005) 26:593–651
DOI 10.1007/s10712-005-1759-6

ELECTRICAL PROPERTIES OF CRUSTAL AND MANTLE ROCKS – A REVIEW OF LABORATORY MEASUREMENTS AND THEIR EXPLANATION

GEORG NOVER
Mineralogisch-Petrologisches Institut, Poppeldorfer Schloss, 53115, Bonn, Germany (E-mail: g.nover@uni-bonn.de)

(Received 1 April 2003; Accepted 26 July 2004)

Abstract. The electrical properties of rocks and minerals are controlled by thermodynamic parameters like pressure and temperature and by the chemistry of the medium in which the charge carriers move. Four different charge transport processes can be distinguished. *Electrolytic* conduction in fluid saturated porous rocks depends on petrophysical properties, such as porosity, permeability and connectivity of the pore system, and on chemical parameters of the pore fluid like ion species, its concentration in the pore fluid and temperature. Additionally, electrochemical interactions between water dipoles or ions and the negatively charged mineral surface must be considered. In special geological settings *electronic* conduction can increase rock conductivities by several orders of magnitude if the highly conducting phases (graphite or ores) form an interconnected network. Electronic and electrolytic conduction depend moderately on pressure and temperature changes, while *semiconduction* in mineral phases forming the Earth's mantle strongly depends on temperature and responds less significantly to pressure changes. Olivine exhibits thermally induced semiconduction under upper mantle conditions; if pressure and temperature exceed $\sim$ 14 GPa and 1400 °C, the phase transition olivine into spinel will further enhance the conductivity due to structural changes from orthorhombic into cubic symmetry. The thermodynamic parameters (temperature, pressure) and oxygen fugacity control the formation, number and mobility of charge carriers. The conductivity temperature relation follows an Arrhenius behaviour, while oxygen fugacity controls the oxidation state of iron and thus the number of electrons acting as additional charge carriers. In volcanic areas rock conductivities may be enhanced by the formation of *partial melts* under the restriction that the molten phase is interconnected. These four charge transport mechanisms must be considered for the interpretation of geophysical field and borehole data. Laboratory data provide a reproducible and reliable database of electrical properties of homogenous mineral phases and heterogenous rock samples. The outcome of geoelectric models can thus be enhanced significantly. This review focuses on a compilation of fairly new advances in experimental laboratory work together with their explanation.

Keywords: electrical conductivity, minerals, pressure, rocks, temperature

1. Introduction

Geophysicists have used different electrical methods for the determination of the electrical structure of the Earth's crust and mantle. Magnetotelluric (MT) measurements revealed that the Earth's continental crust contains zones of high electrical conductivity (Haak and Hutton, 1986) and provided evidence that the structure of the crust is not simply layered but varies laterally and with depth (Campbell, 1987). Various models and hypotheses were suggested to explain such electrical inhomogenities. A common feature of these models is that they all have to fit different aspects that control the electrical properties; thus the models differ in space, time and scale. Even on a local scale crustal and mantle rocks exhibit a broad variety in composition, thus reflecting the geological and tectonic history and their influence on certain properties, e.g., rheology, heat flow, water saturation, grain size, pores and fractures. Taking further into account the environmental conditions at a given depth, thermodynamic properties like pressure and temperature or oxygen fugacity have to be considered regarding their influence on electrical rock properties.

Upper crustal rocks exhibit pores and fractures that may be partially or totally filled with fluid electrolytes. Electrical charge transport in these rocks is an *electrolytic process* and thus is controlled by the geometry (e.g., porosity, aspect ratio, tortuosity, degree of interconnection) of the pore system (Section 3.1). The chemistry of the pore electrolyte can vary from low to high salinities of up to more than 150 g NaCl per litre. Consequently, the electrolyte chemistry is the most important factor for charge transport in fluid saturated crustal rocks. Besides electrolyte conductivity, electrochemical interactions between the fluid electrolyte and the mineral matrix contribute additionally (surface conductivity, Section 4.1.1) to the total conductivity.

In special geological situations electronic charge transport through highly conducting phases, like graphite, may occur. High electrical conductivity in thrust fault structures is assumed to be caused by *electronic conduction* through interconnected graphite films (Sections 3.2 and 4.2). This is still under debate because electrolytic conduction through an open and well-interconnected pore system may explain highly conducting zones as well, a model that is favoured by various groups. Progress towards a solution of this problem has been complicated by the lack of accurate knowledge of the composition of the crust and by the lack of relevant and reliable laboratory data on mid- and lower-crustal rocks. This is mainly due to the difficulty of attaining simulated lower crustal conditions in the laboratory high-pressure, high-temperature (HPHT) experiments.

At lower crustal and upper mantle pressure and temperature conditions, temperature-induced *semiconduction* is the dominant transport mechanism. As long as phase transitions can be neglected (Section 4.3.2), measured

conductivities are weakly dependent on pressure and strongly dependent on temperature and oxygen fugacity (oxygen partial pressure). The latter quantity is of special importance for a reducing or oxidising environment and thus controls, e.g., the number and charge of charge carriers, e.g., iron (Fe^{2+}, Fe^{3+}). Measurements of the electrical conductivity of typical mantle mineral phases like olivine and pyroxene were studied intensively (Sections 3.3 and 4.3.1) in the past. Today, conductivity measurements are performed in sophisticated HPHT laboratory experiments (Section 4.3) using piston-cylinder, belt and multi-anvil devices. Such experiments allow the observations of charge transport under mantle conditions, and the control and measurement of the influence of thermodynamic and chemical parameters, e.g., temperature, pressure and oxygen fugacity on temperature-induced semiconduction, to be investigated. Due to the high p,T conditions required for such experiments, it is critical to ensure thermodynamic equilibrium or stationary conditions for one experimental cycle. These experimental problems are the main cause of the scatter in conductivity data reported by various groups in the past. The most crucial point is the measuring time required for each change in temperature to reach stationary conditions. In many experimental setups an inefficient cooling system impedes long-term temperature measurements. Without a cooling system being applied, electrical conductivity measurements were performed rather fast (in a few hours) under non-equilibrium conditions. But, as we know today, thermodynamics require long-term measurements (up to weeks) to ensure stationary conditions. A further complication is due to the fact that laboratory measurements are generally performed on powder samples. Their results differ slightly (even when the thermodynamic parameters are controlled) from single crystal measurements where the conductivity was measured in the direction of the three crystallographic base vectors defining the unit cell. This is mainly caused by the grain size, by recrystallisation and the growth of grains at the given experimental p,T conditions, and by different conductivity and charge transport in the three directions. For laboratory data to be of use for electrical modelling the experimental boundary conditions have to be achieved. This assures that long reaction times can be established for each change in temperature to ensure that the conductivity data were measured under stationary thermodynamic conditions.

In volcanically active environments, temperatures at shallow depths are sufficiently high to produce local conductivity anomalies. These may be explained by the formation of *partial melts* if the temperature is above the solidus line (Sections 3.4 and 4.4). The conductivity of the melt is much higher than that of the solid rock and, if the melt forms an interconnected fluid phase covering the grains, then a significant increase in conductivity can be measured. This kind of charge transport can be assumed in areas where

temperature gradients are sufficiently high (volcanic areas) or at greater depth in the Earth's mantle.

In the last 10 years HPHT techniques were improved significantly by the use of more sophisticated pressure cells. Autoclaves allow the control and individual regulation of pressure, stress, temperature and fluid-pressure. These new developments enabled the measurement of electrical rock properties under simulated *in-situ* conditions (Sections 2 and 4). Solid state pressure cells like multi-anvil devices allow the measurement of X-ray diffraction, acoustic velocities and electrical properties under *in-situ* conditions while simultaneously pressure, temperature and strain are applied. Electrical properties are generally measured as frequency dependent complex impedances. Physical and chemical parameters that may constrain the transport of electrical charges thus are accessible when frequency dependent complex electrical conductivity measurements are performed instead of fixed frequency measurements. This technique allows an interpretation of electrical data in terms of charge carrier transport models and thus makes conductivity data much more reliable.

Many research papers and review papers have been published giving a thorough overview of the physical and chemical parameters that control the electrical charge transport in rocks and minerals (Olhoeft, 1976; Olhoeft, 1979; Cemic et al., 1980, 1981; Duba et al., 1974, 1982, 1994; Glover and Vine, 1995; Glover et al. 1996; Hinze et al., 1981, 1982; Revil et al., 1996; Ruffet et al., 1991, 1995). Within the last 10 years many efforts were concentrated on the application of more sophisticated techniques to get a deeper insight into the physical and chemical parameters that control the electrical charge transport. Laboratory measurements provide accurate data of electrical charge transport, the physical background of transport mechanisms for rocks under elevated p,T conditions, and thus can be used for upscaling laboratory data to larger geological units in order to constrain geophysical models and to explain electrical structures and discontinuities in the Earth's crust.

This review paper considers only fairly recent publications on the electrical properties of crustal rocks and Earth mantle minerals. Papers dealing with other analytical techniques like X-ray diffraction, IR and UV spectroscopy and acoustic velocities are not considered though they provide valuable information on rheological properties, phase transformations, density and pore space, data that are essential for the understanding of processes in, e.g., a subducting slab.

This paper is organised in five sections, starting with this introduction (Section 1); it is followed by an experimental section (Section 2) where aspects of HPHT techniques and the theoretical background are described. In Section 3 the principles of the electrical charge transport (electrolytic, electronic, semiconduction and partial melts) in crustal rocks and mantle minerals are discussed. This is followed by Section 4 where the data of

important papers are presented in more detail. Section 5 summarises the most important results out of a large number of publications available; only those that explain the principal effects of charge transport in crustal and mantle rocks are given.

2. Experimental studies and their interpretation

One objective of laboratory experiments is to measure the physical properties of minerals and rocks from the Earth's surface p,T conditions down through the mantle to even core conditions. This requires the use of HPHT devices that are designed to allow measurements in a certain pressure and temperature range (Figure 1). Four different devices are used to study samples from the surface to the Earth's core p,T conditions. These devices may differ in their construction due to special requirements that are needed to measure, e.g., electrical and hydraulic properties or acoustic velocities.

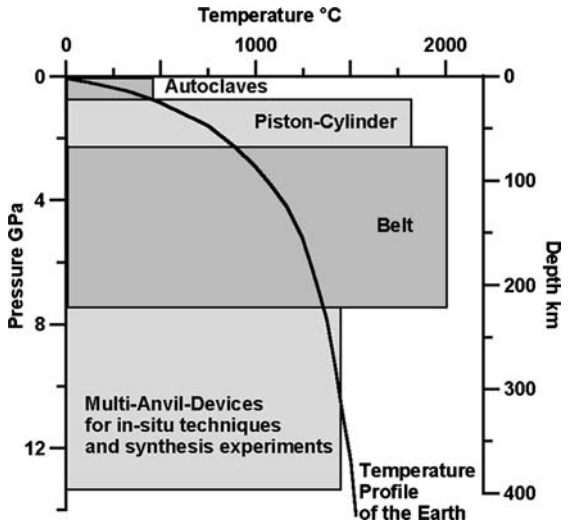

Figure 1. Diagram of the temperature (T), pressure (p) and depth profile of the Earth and the HPHT equipment used in this p,T-range. Autoclaves are used for studies to 400 MPa. Piston-cylinder apparatus is designed for the temperature and pressure range up to 1600 °C and 4 GPa; sample sizes are in the range of 100 mm in diameter and up to 10 mm height. Belt apparatus can be operated up to 8 GPa and temperatures of up to 1900 °C. Sample dimensions in such research facilities are in the range of 4 mm in diameter and 4 mm height and for industrial diamond synthesis in the range of some cm. Multi-anvil-devices of hexaedral geometry allow pressures of up to 12 GPa. Temperatures can be increased up to 1800° C. The dimensions of the cylindrical shaped samples depend on piston size, and range from a few mm up to cm. Diamond squeezers are in use for studies in the mega-bar range. The samples are less than 10μm, temperatures are applied using laser-heating techniques. Detailed information on the HPHT equipment can be obtained from the homepage www.min.uni-bonn.de.

2.1. HPHT EQUIPMENT

Using pressure as the criterion for classification, at low-pressure conditions fluid or gas operated steel ***autoclaves*** are used in the pressure range of up to 1 GPa. These devices allow measurements on large-scale samples up to standard drill core dimensions. Additional features of these autoclaves are the independent variation of hydrostatic (confining) pressure, the application of differential pressures and the controlled variation of pore pressures to simulate environmental conditions to a depth of >10 km in laboratory experiments. Measured data can be directly compared with borehole data of that depth if upscaled. Temperatures are generally limited by the annealing temperature of the steel construction as long as no cooling system is installed.

Solid state pressure techniques of the *piston-cylinder* type (cylindrical geometry of the pistons) and (conical) *belt* type apparatus are used for generation of pressures greater than 2 GPa. The piston cylinder technique is operated up to about 4 GPa, and belt-types up to 8 GPa. When combined with a cooling system both devices allow long time measurements at temperatures >1400 °C for weeks. If the pressure gradient across the sample does not exceed 0.2 GPa and temperature gradients are less than $< \pm 10$ to 15 °C at about 1600 °C then the dimensions of a cylindrical sample are limited to roughly 1/3 of the piston diameter and 1/6 of the height for piston-cylinder devices.

Sample diameter and height for the *belt apparatus* are directly related to the dimensions of the conical pistons. The diameter of the inner conical drill hole in the tungsten carbide matrix can range from several mm up to some cm, depending on the process for which it is designed. For industrial diamond synthesis diameters of up to 10 cm are in use, whereas for research diameters in the range of 1–3 cm are convenient. This still allows sample geometries comparable with those of the piston-cylinder forms of 3 up to 10 mm in diameter. Temperatures can be increased up to a maximum value of 2000 °C while the gradient is still $< \pm 15$ °C from top to bottom of the sample. The accuracy of the temperature readings is better than 1 °C.

If pressures above 8–10 GPa are required, *multi-anvil devices* of tetrahedral, hexahedral or octahedral geometry are used. These types of HPHT forms can be operated in single stage mode or double stage mode, thus allowing the application of pressures of up to 25 GPa. Experimental temperatures are comparable with those of the belt-type machines, but experimental times are limited to a few hours reaction time due to inappropriate cooling systems. If the physical properties of samples have to be studied under *in-situ* conditions, the single stage technique is used. Machines of this type found at research facilities all over the world are often operated in combination with a synchrotron radiation source that enables energy dispersive X-ray diffraction (EDX) as well as angle dispersive X-ray diffraction

observations. X-ray diffraction studies can be performed in parallel with electrical conductivity measurements. Thus phase transitions of, e.g., mantle mineral phases or partial melting can be followed under *in-situ* pressure and temperature conditions using X-ray diffraction and electrical conductivity data.

In the Mbar pressure range, *diamond anvil* techniques (diamond-squeezers) are the appropriate tools. These pressure cells have the advantage that diamonds are transparent from IR to UV and X-rays and thus allow phase transitions to be studied under very high p,T conditions. Heating of the sample is still a problem due to inefficient energy absorption of the samples. In principle laser-heating and optical temperature measurements are sophisticated methods for precise temperature measurement and control. Sample sizes are in the range of a few microns depending on the size of the flat of the diamond that is in the range from roughly 600 μm down to less than 100 μm. The two diamonds are separated by a gasket. A drillhole in the gasket contains the sample, pressure marker and a pressure transducing fluid phase; its diameter ranges from >300 down to <50–100 μm for the highest pressures. This technique is used to study, e.g., materials at lower mantle and even Earth's core p,T conditions.

2.2. Frequency dispersion measurements in HPHT devices

Frequency dependent complex electrical impedance measurements performed in HPHT devices generate many problems that have to be controlled or minimised. These problems are caused by the metallic environment, electrical lead through, and the noise due to the resistance heating system that generally requires low voltage but high currents of up to some hundreds of Amperes. Further restrictions result from the sample holder, the sample electrode interface and the cable connectors with the consequence that the frequency range accessible in experiments is limited. Stray capacitances and inductances have to be considered when the experimental data are interpreted by fitting model data to the measured data in order to derive a physically and chemically reasonable interpretation of the complex electrical response of the rock sample under test.

To minimise such experimental problems, different kinds of electrode arrangements are in use. Their application depends on the pressure and temperature range under which the experiments have to be performed. At low pressures and temperatures 4-electrode techniques are easy to install. Current electrodes are placed on the end faces of a cylindrical sample and the voltage drop is recorded by two field electrodes. Thus there is no disturbance of the recorded signal due to electrode polarisations.

In solid state pressure devices the guard ring technique is used to measure electrical properties of samples under conditions of elevated pressure and temperature. The resistance graphite heating system causes stray fields that

have to be shielded. A proper shielding in combination with a narrow band lock-in-analyser allows the measurement of the frequency dependence of the complex sample response in a noisy environment. Nevertheless electrode polarisations dominate the complex response at frequencies below roughly 1 kHz.

Two-electrode techniques are applied when fluid saturated porous rock samples have to be measured under crustal p,T conditions. Again, the low frequency limit is 1 kHz, while the high-frequency limit is about 1 MHz due to coupling and cable effects. As electrodes various materials like stainless steel, graphite, platinum, gold, silver and copper, as well as porous electrodes, are widely used. Cable capacitances and inductive coupling can roughly be considered by measuring an equivalent circuit with similar values of resistance and capacitance to the sample under test. Theoretical calculation of the complex response and comparison with the measured complex response gives an estimate to correct for the inductive and capacitive coupling effects. If only moderate pressures are applied and the temperatures are not too high, non-polarisable electrodes like Ag–AgCl or Hg–HgCl are used to measure the conductivity of fluid saturated sedimentary rocks.

2.3. Theory of complex impedance measurements

The electrical charge transport in geo-materials is based on electrolytic conduction, electronic conduction, temperature-induced semiconduction or ionic transport in a molten phase. If an electric field is applied to such a system a marked frequency dependence of the electrical parameters of conductivity and permittivity is observed. This is caused by a conduction current and a displacement current. Displacement currents are due to polarisation mechanisms like electronic polarisation, atomic polarisation, orientation polarisation, electrode polarisation and membrane polarisation (Figure 2).

The electrical properties of materials are characterised by the parameters resistivity $\rho(\Omega\ \mathrm{m})$ (or its reciprocal, the conductivity $\sigma = 1/\rho$ (S/m)) and the dielectric permittivity ε (F/m). These quantities define the conduction current density $\mathbf{J}$ being caused by an electric field $\mathbf{E}$ and the electric displacement $\mathbf{D}$, where

$$\mathbf{J} = \sigma\mathbf{E} \tag{1}$$

and

$$\mathbf{D} = \varepsilon\mathbf{E} \tag{2}$$

The dielectric constant ε_r (or relative dielectric permittivity) of the medium is defined as

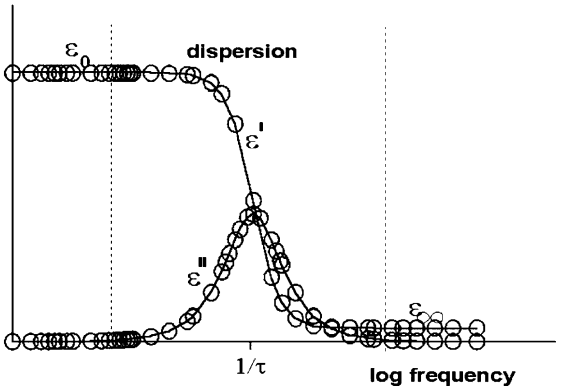

Figure 2. Dispersion, the frequency variation of dielectric properties. ε_∞ is the optical, ε_o is the static, and ε', ε'' are the real and imaginary parts, of the dielectric constant.

$$\varepsilon_r = \varepsilon/\varepsilon_0, \tag{3}$$

where $\varepsilon_0 = 8.854 \times 10^{-12}$ F/m is the dielectric permittivity of free space. Rock forming minerals exhibit conductivity and polarisability. As a consequence, an applied electric field causes both a conduction current and a displacement current to flow; these are out of phase with each other. Conductivity, resistivity and permittivity are thus complex and also frequency dependent (Fuller and Ward, 1970). Therefore,

$$\sigma^*(\omega) = \sigma'(\omega) + i\sigma''(\omega) \tag{4}$$

$$\rho^*(\omega) = \rho'(\omega) + i\rho''(\omega) \tag{5}$$

and

$$\varepsilon^*(\omega) = \varepsilon'(\omega) + i\varepsilon''(\omega), \tag{6}$$

where ω is the angular frequency $\omega = 2\pi f$, f being the frequency; $i = \sqrt{-1}$. Primed quantities are the real parts and double primed are the imaginary components, respectively. As discussed by Fuller and Ward (1970), the parameters that are actually measured in laboratory and field experiments are not the true values but are effective quantities given by

$$\sigma_{eff}(\omega) = \sigma'(\omega)\omega\varepsilon'' \tag{7}$$

and

$$\varepsilon_{\text{eff}}(\omega) = \varepsilon'(\omega) - \mathrm{i}\sigma''(\omega)/\omega \tag{8}$$

The effective resistivity is

$$\rho_{\text{eff}}(\omega) = 1/\sigma_{\text{eff}}(\omega) \tag{9}$$

The ratio of the imaginary part of any complex quantity to its real part defines the phase angle Φ, e.g., for the effective conductivity in Equation (7),

$$\tan\Phi = [\omega\varepsilon''(\omega)]/\sigma'(\omega). \tag{10}$$

Whereas the real parts of Equations (4) and (6) are often thought of as the 'true' values of the conductivity and permittivity, respectively, the effective quantities in Equations (7) and (8) are the important ones because they are what are actually measured (Fuller and Ward, 1970).

A common way to describe the complex permittivity (or dielectric constant) of natural substances is to use resistor R and capacitor C circuit elements in series and parallel, indicating a relaxation process. Using this scheme, Debye (1927) showed that the complex permittivity $\varepsilon^*{}_{\text{w}}(\omega)$ of water has the frequency dependence given by

$$\varepsilon^*{}_{\text{w}}(\omega) = \varepsilon'(\infty) + [\varepsilon'(\text{o}) - \varepsilon'(\infty)]/(1 + \mathrm{i}\omega\tau) \tag{11}$$

where τ is the time constant of the relaxation phenomenon. The permittivities $\varepsilon'(\text{o})$ and $\varepsilon'(\infty)$ are real, static and high frequency (optical) values, respectively. The static dielectric constant of water is usually taken to be ~ 80 (Figure 2).

The single relaxation process expressed by Equation (11) can be expanded using a distribution of relaxation times differing slightly in time constants, and thus represent a combination array of RC-circuits (Bauerle, 1969; Cole and Cole, 1941; Jonscher, 1975, 1978). Each RC-element describes one relaxation process with the time constant $\tau = \text{RC}$. The complex impedance of this circuit is

$$Z^* = Z' + \mathrm{i}Z'' \tag{12}$$

Various frequency dispersive polarisation processes can be accounted for in this way (Figure 3). Such expressions are valid for simple dielectric media, but they do not adequately describe mixed media like rocks.

2.4. Modelling of complex responses

Simple parallel or series arrays of RC-elements are used to model the frequency dependence of the complex response of electrical charge transport. A conventional method to display frequency dependent complex impedance data is the Cole–Cole diagram where the real part of the impedance Z' is plotted versus the imaginary part Z'' (Figure 4, 5) (Cole and Cole, 1941). The complex response of such a system looks different if the time constants of the relaxations differ by more, or less, than one order of magnitude. Figure 4 shows an example for the complex response of an array of two RC-elements in series where the time constants $\tau_i = R_i C_i$ of the relaxations differ by less than one order of magnitude. This causes an overlapping of the semicircles. In contrast to this Figure 5 shows two well-separated semicircles due to time constants differing by more than one order of magnitude.

The physical interpretation of the intersection of a Cole–Cole semicircle with the real axis at the low-frequency end (right) is a measure of the bulk or volume impedance of the sample. The high-frequency end is found at the origin; frequency varies from low to high frequencies from the right end to the left end of the semicircle. The electronic elements of such an equivalent

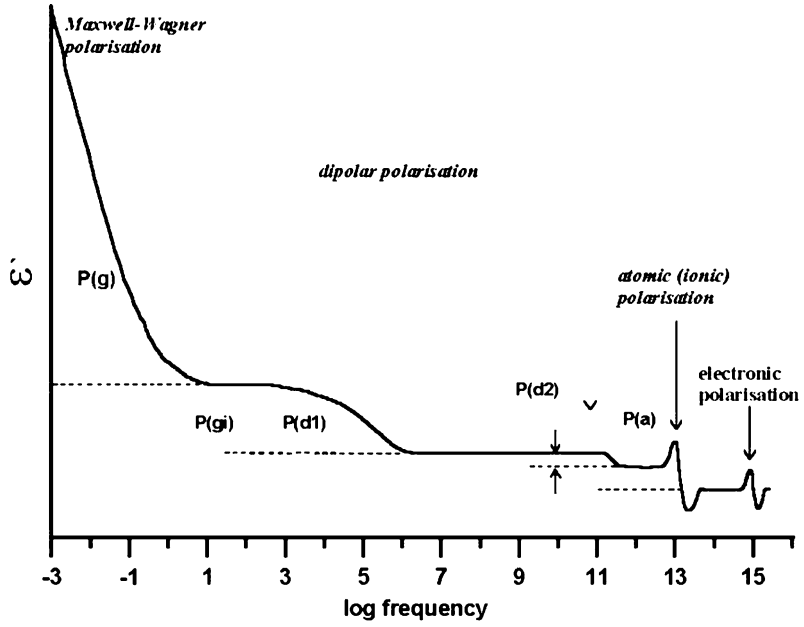

Figure 3. Frequency dependence of the real part of the dielectric constant and corresponding polarisation mechanisms in the frequency range up to 10^{15} Hz. In laboratory experiments the frequency is limited to a few MHz. P_g indicates polarisations of contact areas, P_{gi} are those at grain boundaries, P_d are polarisations due to the orientation of charge carriers, $P_{a,i}$ are ion polarsations and P_e are electron polarisations.

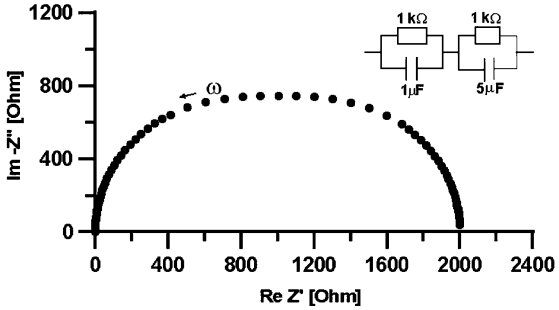

Figure 4. Model calculation of an equivalent circuit of two RC-parallel elements in series. The time constants of the relaxations differ by less than half an order of magnitude, causing overlapping of the semicircles.

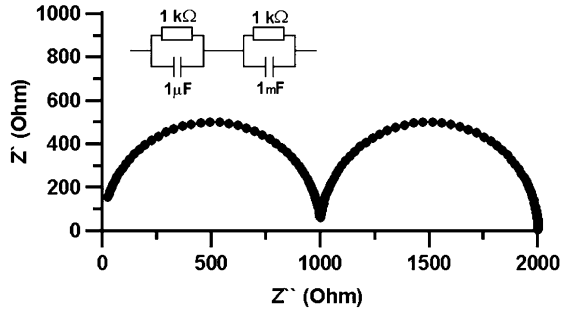

Figure 5. Model calculation with an equivalent circuit of two RC-parallel elements in series. Two well-separated semicircles are visible due to time constants that differ by more than one order of magnitude.

circuit (R1, C1, R2, C2) are related to the physical and chemical parameters of the charge transport model, e.g., R1 and C1 refer to polarisations in the bulk of the electrolyte, while R2 and C2 refer to surface polarisations taking place at the mineral matrix/fluid phase interface layer. Thus the electrolytic charge transport in the bulk of the electrolyte and surface conduction in the electrochemical double layer (DL) can be modelled. Another type of diagram is the Bode-diagram where the absolute value of the impedance $|Z|$ and the phase angle are displayed as a function of frequency (Figure 6).

3. Electrical charge transport in rocks and minerals

3.1. Electrolytic conduction

The electrical properties of fluid saturated rocks depend on composition, microstructure and interfacial effects. A rock sample thus can be considered as a three-component system consisting of grains, pores and interfaces

(Figure 7). The term composition determines the bulk properties of the constituents. These are well known for most rock forming minerals and pore fluids. Microstructure considers the way in which these properties are averaged over a larger volume, thus taking into account the geometrical arrangement of the constituents. They are governed by the geological history of the rock, namely sedimentation conditions and metamorphic overprint. Anisotropies in petrophysical properties like porosity, permeability, crack orientation, tortuosity and texture, etc. may thus be caused. Interfacial effects are due to mineral/fluid interactions which result in the formation of the electrochemical DL. This layer is particularly important for the electrical properties of clay bearing rocks and in tight rock samples. Interfacial effects depend on the chemistry of the pore electrolyte like ionic concentration, ionic species and the surface charges of the rock forming minerals that interact with the pore fluid.

Based on DC conductivity data, Archie (1942) proposed an empirical equation that relates the rock conductivity σ_r (of mainly sandstones) to the conductivity of a pore saturating fluid σ_f. The rocks were assumed to exhibit intergranular porosity, and no disturbances due to the presence of reactive

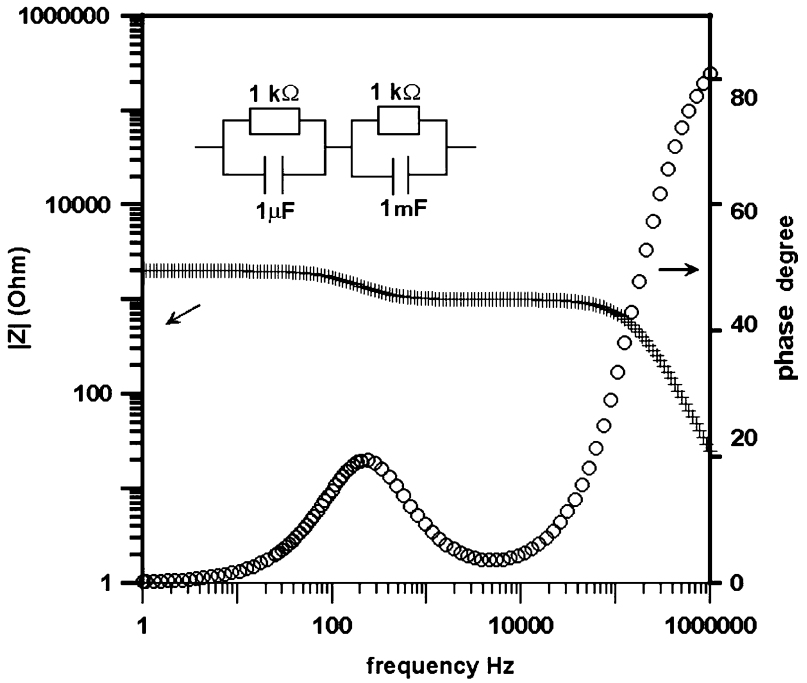

Figure 6. Model calculation of a two-stage relaxation process. The absolute value of the impedance $|Z|$ and the phase angle are displayed as a function of frequency; this is termed a Bode plot.

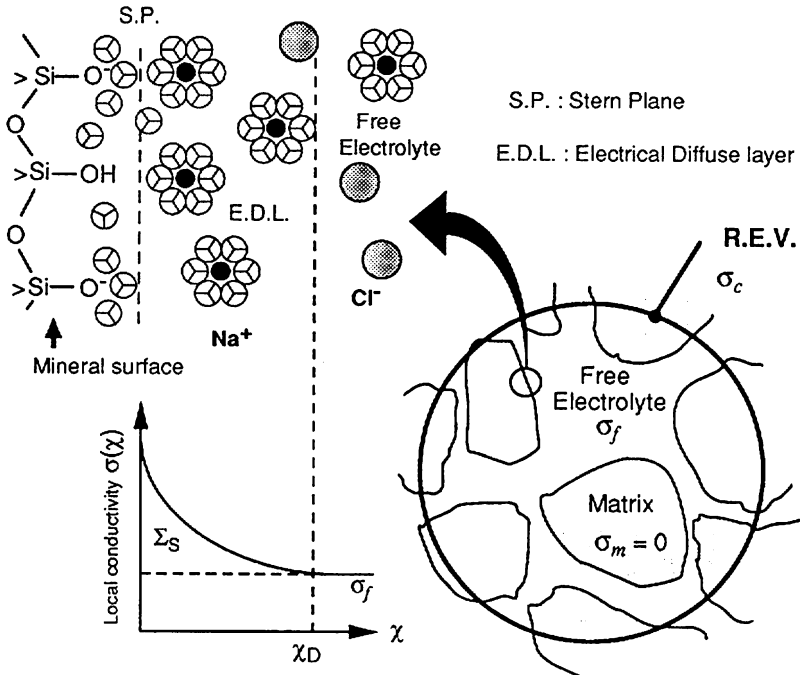

Figure 7. Schematic representation of the electrical DL on a mineral surface (Revil et al., 1996). The parameter σ_c is the effective conductivity of a representative elementary volume (REV), whereas σ_f and σ_m are the free electrolyte and matrix conductivity. The disturbed conductivity in the electrical diffuse layer can be taken into account by a specific conductance parameter Σ_s.

minerals such as clay were considered. The ratio of σ to σ_s is termed the formation factor F. The conductivity of an electrolyte is a function of salt concentration (molarity), ion charge (Equation (13)) and temperature (Equation (14)):

$$\sigma_f = \Sigma(C_a \cdot \upsilon_a \cdot f_a + C_c \cdot \upsilon_c \cdot f_c) \tag{13}$$

$$\sigma_{f(T)} = \sigma_f(20C) \cdot (1 + 2.16 \times 10^{-2}\Delta T + 8 \times 10^{-6}(\Delta T)^2) \tag{14}$$

where C_a, C_c are the concentrations of the anions and cations, v_a, v_c are the mobilities and f_a, f_c are the conductivity coefficients depending on the concentration and chemical composition and ion charge (Ruffet et al., 1995), and with ΔT being the difference of temperature from 20 °C (Dachnov, 1975).

Following the argument above that a rock sample can be considered as a three-component system, then the total conductivity σ_t of a fluid saturated

rock is the sum of electrolyte conductivity σ_f and surface conductivity σ_m as long as the contributions of charge transport through the mineral matrix can be neglected. With the restriction that $\sigma_f >> \sigma_m$, the total conductivity is defined by equation 15:

$$\sigma_t = \sigma_f + m \cdot (1 + \theta^m) \cdot \sigma_s \cdot \theta^m \tag{15}$$

where m is the cementation exponent and θ the porosity (Waxman and Smits, 1968; Pape et al., 1981, 1999; Johnson and Sen, 1988; Bernabe 1986, 1988; David and Darot 1989; Nover et al., 1995; Roberts et al., 2001; Roberts, 2002). Surface conductivity effects are well known for shale formations, or at low salinities, or in low-porous, low-permeable rocks.

The electrochemical DL is a result of fluid–solid interactions. Clay minerals, e.g., exhibit a strong negative electrical field perpendicular to the surface due to charge deficiencies at the surface of the crystal lattice. This negative field attracts cations and repels anions. This zone near to the clay surface, where counterions are concentrated, constitutes a layer with a specific conductance. Its outer surface defines the Stern Plane; surface conductivity takes place in this layer. Beyond the Stern Plane hydrated anions and cations as well as water dipoles are found in the electrical diffuse layer (Figure 7). Interactions with the charged mineral surface are less pronounced. Both layers, the Stern layer and the electrical diffuse layer, form the electrochemical DL. The thickness of the DL depends on the species of ions adsorbed and thus on the chemistry of the electrolyte. It decreases when the ion concentration increases. The Gouy Chapman model of the DL assumes a charge distribution in the diffuse layer following a Boltzmann distribution. Thus the potential drop from the surface into the bulk of the electrolyte can be characterised by the Debye length, being a measure of the thickness of the DL. The Debye length is the distance beyond which the interface effect is screened. As the thickness of the DL decreases with increasing salinity (molarity of the pore fluid), the electrolyte molarity is an indirect measure of the thickness of the DL. The surface conductivity σ_s is proportional to the surface charge density Q_s of the rock forming minerals and the 'strength' of the interaction between the solid phase and the ions in the electrolyte (Revil et al., 1996).

Frequency dependent complex conductivity measurements lead to the conductivity and the dielectric properties of the system rock/fluid as a whole. The important effect is the enhancement of the dielectric constant at low frequencies (Fuller and Ward, 1970; Knight and Nur, 1987). At low frequencies, very high-relative permittivities (up to 10^4) were measured in mineral–water mixtures, though the constituents exhibit relative permittivities in the range of 5–80. This behaviour is of particular importance for clay–water mixtures (Olhoeft, 1987) that were the starting point for the detailed studies of interfacial effects and surface conductivity (Ruffet et al., 1995; Börner and

Schön, 1995; Revil et al., 1996). Ruffet et al. (1995) and Revil et al. (1996) studied surface conductivity σ_s in detail and presented an equation considering the electrochemical dependencies:

$$s \int_0^{(\chi^D)} (\sigma(\chi) - \sigma_f) \tag{16}$$

$\sigma(\chi)$ is the spatially varying conductivity in the electrical diffuse layer and χ measures the distance along a normal directed into the pore space from the Stern Plane. It converges to σ_f, the electrolyte conductivity, for a distance from the mineral surface representing the free electrolyte; $\sigma(\chi)$ depends mainly on the concentration and type of electrolyte, its charge, temperature and the thickness χ_D the Debye (1913) screening length of the electrical diffuse layer that is a part of the electrochemical DL. Equation (16) is valid for a system under stationary (equilibrium) conditions where no pressure or electrical gradient causes a movement of the fluid phase. If a movement is considered this would require the introduction of the Zeta-potential (ZP) that can be measured either by electrophoretic or electro-osmotic techniques, depending on which species is the moving one. The electro-osmotic ZP is based on velocity measurements of dispersed minerals with sizes of a few μm in an electrolyte.

Except for some special experimental set-ups in well-defined chemical environments, most of the parameters are not known. Consequently the surface conductivity term can only be expressed by a general factor shifting the conductivity to higher values. Thus the bulk conductivity σ_{bulk} of a sample was expressed by a sum of the various contributions to the total conductivity:

$$\sigma_{\text{bulk}} = \sigma_f + \sigma_m + \sigma_s \tag{17}$$

where σ_f is the electrolyte conductivity, σ is the matrix conductivity of the rock forming minerals (low in the case of pure quartz, but high in the presence of clay) and σ_s the surface conductivity caused by polarisation of, e.g., ions or hydrated ions at the inner surface of the pore system. In principle, different polarisations in such a system are characterised by different time constants, which can be identified by studying the frequency dependence of the system rock/pore saturating brine (Olhoeft, 1985).

3.2. Electronic conduction

Electronic conduction may increase the electrical conductivity by orders of magnitude if the highly conducting phases (graphite, ores) form an interconnected network. The conductivity of such a system can be described using

Ohm's law. A limiting condition is given by the degree of interconnection and the specific conductance of the metallic conducting phases. If not interconnected, they can be assumed to be good conductors in an isolating matrix; otherwise, variations in the degree of interconnection can be calculated using, e.g., the upper bound formula of Hashin and Shtrikman (1962). The most prominent candidate for a conductivity increase is carbon (graphite). Duba and Shankland (1982) used the upper bound formula to calculate the absolute amount of well-ordered graphite required to enhance the conductivity of dry rocks. They found that a volume fraction of carbon of only 5×10^{-6}% can cause a conductivity of 0.1 S/m if well interconnected.

The origin and transport of carbon is still controversial; passive or active enrichment in crustal rocks are both considered, but the thermodynamic parameters that control precipitation (reduction, oxidation) of carbon from a gas or a fluid phase, e.g., CO_2 or CH_4 are not well understood. If organic carbon is assumed to be the carbon source, the well known processes of coalification and, subsequently, that of graphitisation of hard coal can be used to estimate the p,T conditions under which graphite may be formed. Greenschist facies p,T conditions were found to be sufficient to transform poorly conducting carbon into highly conducting graphite ($p <$ 0.6 MPa, $T < 500$ °C; Nover and Stoll, 2005). However if a carbon-rich gas like CO_2 or CH_4 is assumed to be the carbon source, what is the process which provides the required activation energy to reduce or oxidise these compounds under lower crustal conditions? The first ideas (Mogk and Mathez, 2000) and experiments were proposed and performed by Roberts et al. (1999), who observed an increase in conductivity on newly formed fractured surfaces in presence of a CO_2 atmosphere.

3.3. Semiconduction

Most rock forming minerals act like insulators at room temperature and thus their electrical conductivity is rather low. This picture is changed when the temperature is increased and semiconduction takes place due to the enhanced mobility of lattice defects and impurities. The number and mobility of these charge carriers determine the conductivity σ that can be described in general as:

$$\sigma = \Sigma e q_i n_i v_i \tag{18}$$

where e is the charge of an electron, q_i the number of charges of the carrier i, n_i the concentration and v_i the mobility of the charge carriers. Mobility and concentration both follow an exponential law:

$$c_i = c_i^{\circ} \exp -G^*_{f,i}/kT \tag{19}$$

$$v_i = v_i^{\circ} \exp -G^*_{m,i}/kT \tag{20}$$

where c_i° is concentration of the charge carrier i for $T \rightarrow \infty$, v_i° the mobility of charge carrier i for $T \rightarrow \infty$, $G^*_{m,i}$ the free enthalpy required to move a charge carrier i, $G^*_{f,i}$ the free enthalpy to generate a charge carrier i, k Boltzmann's constant, and T the temperature in Kelvin. Charge carriers can be moved by two different processes; at low-temperatures impurities on interstitial lattice positions can be moved causing extrinsic charge transport, whereas at high temperatures ions of the crystal lattice can move from regular places to interstitial positions, thus causing intrinsic conduction. Consequently the conductivity of an ionic crystal σ_{ges} can be defined as the sum of exponential terms (Figure 8):

$$\sigma_{\text{ges}} = \sigma_1 \exp(-E_1/kT) + \sigma_2(-E_2/kT) + \cdots + \sigma_i \exp(-E_i/kT) \tag{21}$$

The terms E_1, E_2, E_i are the individual free enthalpies that are combined to one activation energy that is required for the formation and the movement of the charge carriers. Extrinsic and intrinsic defects generally can be assumed to contribute to the total conductivity. The defect concentration depends exponentially on the enthalpy of formation, whereas the mobility of charges depends on the geometry of the crystal lattice and thus is a tensor function with a significant anisotropy in conductivity. σ_{ges} was measured on single crystals of olivine by Schock et al. (1989) and Wanamaker and Duba (1993), whereas powder samples exhibit a mean conductivity. In olivine the most probable defects are extrinsic defects due in part to excess Mg on unoccupied octahedral positions in the lattice, and charge that is balanced by electrons or defect-electrons. Intrinsic defects were generated by increasing temperature, causing Mg–Frenkel defects. Regular Mg-ions moved to interstitial positions leaving back 2-fold negative vacancies.

Temperature-induced semiconduction depends on the thermodynamic parameters of temperature, pressure and oxygen fugacity. All of these directly influence the defect concentration and its equilibrium which is different for each given temperature. Thus the temperature dependence of the conductivity can be described by an Arrhenius-like behaviour:

$$\sigma = \sigma_{\text{o}} \exp(-E_{\text{a}}/kT) \tag{22}$$

where σ is the conductivity, σ_{o} a pre-exponential factor, and E_{a} the activation energy. The activation energy can be calculated from a plot of log conductivity against reciprocal temperature. The slope of the log σ versus $(1/T)$ dependence is equal E_{a}/k, and thus gives an estimate of E_{a}. In general two

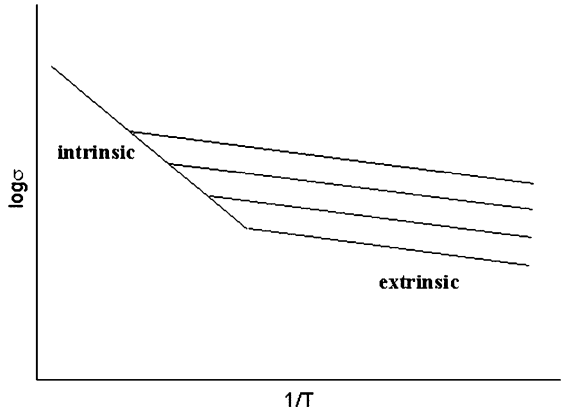

Figure 8. Schematic representation of an Arrhenius diagram where log conductivity is plotted against the reciprocal of the absolute temperature. The four lines represent different extrinsic charge transport processes, typical for temperature-induced semiconduction. The variation of the gradient at elevated temperatures indicates that intrinsic charge transport then dominates the conduction process.

regions different in activation energy could be detected in the temperature range from 500 up to 1500 °C for mantle relevant mineral phases, representing extrinsic and intrinsic conduction (Figure 8) (Cemic et al., 1980; Duba et al., 1974, 1982, Schock et al., 1989; Hinze et al., 1981, 1982; Roberts and Tyburczy, 1993a, 1993b). Activation energiess for the two transport processes range for olivines from 1 to 5 eV.

3.4. Partial melts

Partial melts also may increase the electrical conductivity by several orders of magnitude if the temperatures are sufficiently high. These processes play a key role in crustal and mantle dynamics and their evolution. The temperature at which partial melts may form depends on the chemistry of the rocks, the presence of hydrous mineral phases or the presence of free water (Roberts and Tyburczy, 1999; Poe et al., 2001). These parameters define the position of the solidus in a p,T diagram. Laboratory experiments on such systems are complicated by non-equilibrium conditions between the melt phase and the remaining solid rock when temperatures are changed. This non-equilibrium between the fluid and solid phase will directly affect the concentration of the ions in the fluid phase and thus the number of charge carriers. The electrical signature of a partial melt can be seen in the complex response of the sample when the frequency dependence of the conductivity diminishes (Figure 9). If a melt phase is formed, the conductivity is enhanced by several orders in magnitude (Shankland and Waff, 1977; Schilling et al., 1997, 2001; Roberts

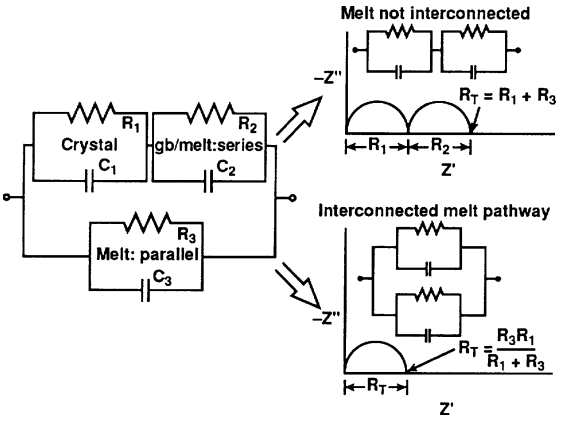

Figure 9. Equivalent circuit and schematic responses of three conduction mechanisms: crystal, grain-boundary/melt series, and melt parallel, and a representative electrical circuit showing one possible combination of the three mechanisms. The upper right response indicates that series conduction is dominant; the lower diagram indicates that parallel conduction is dominant (Roberts and Tyburczy, 1999).

and Tyburczy, 1999; Bagdassarov et al.,2002; Partzsch et al., 2000; Maumus et al. 2001; Poe et al., 2001; Nover et al., 2004a, 2004b, 2006).

4. Results

4.1. Electrolytic condition

In this section, only those papers that deal with specific aspects such as surface conductivity, complex impedance measurements, pressure and stress dependence of the conductivity are considered, as also are those papers that deal with a relation between electrical model and measured data. Papers that only describe the electrical properties of rocks from specific locations are not considered in this review.

4.1.1. *Surface conductivity*

Knight (1991) measured the conductivity of sandstones during water takeup and drainage. A significant hysteresis in conductivity was detected, showing that the conductivity depends on the saturation history of the sample. Conductivity changes reflect variations of fluid and air distribution on the pore scale as caused by natural saturation processes such as infiltration and evaporation. This observation was explained by the number of monolayers of water that coat the inner surface of the pores and conduction at the air/water interface, parameters that are very important in characterising transport in the unsaturated zone.

Vanhala and Soininen (1995) used the spectral induced polarisation response measured over the frequency range from 0.01 up to 1000 Hz to compare laboratory results with field measurements. They measured the resistivity spectrum of various soil samples having different mineralogy, grain size distribution, moisture content and electrolyte composition under saturated and unsaturated conditions. They found differences in the complex response in the low frequency region due to polarisable and non-polarisable electrodes, but easy to use platinum or steel electrodes produce reliable results in the frequency range of 0.016 up to >1000 Hz. The maximum phase shift due to surface polarisations was detected below 0.1 mrad, with high input impedances >100 MΩ and sample resistances <10 MΩ. As expected the phase spectra of various silt, sand and till samples were not critically sensitive to the sampling and preparation of the samples (Figure 10) due to the unconsolidated nature of the glacial sediments. The laboratory data could be correlated with induced polarisation (IP) field data of glacial soils.

Dielectric dispersion measurements were used by Haslund and Nost (1998) to calculate the porosity and formation factor of sintered porous glass samples. A bimodal grain shape distribution allowed a reasonable fit to the measured dispersion data. The good agreement of the refined parameters and measured data using the pore fluid conductivity, porosity and two geometric quantities as adjustable parameters allowed both porosity and formation factor to be derived for the synthetic sintered glass sample, using the theory of Mendelson and Cohen (1982) and Sen (1981, 1984) (MCS). In Figure 11 experimental points and theoretical curves for the normalised effective conductivity σ/σ_w of various samples are displayed versus normalised frequency ω/ω_w on a logarithmic scale. The angular frequency ω has been normalised by the relaxation frequency of the ionic conduction in water $\omega_w = \sigma_w/(\varepsilon_o \varepsilon'_w)$. The close fit shows that the (MCS) model allows porosity and formation factor to be predicted for the sintered glass specimens when petrophysical properties like porosity, aspect ratio and pore-electrolyte conductivity were variable in the fitting procedure.

Glover et al. (1994) report on conductivity measurements performed on sandstones saturated with a range of different types and concentrations of fluid electrolytes in the frequency range from 20 up to 1 MHz. Two regimes of conduction could be separated. At high electrolyte salinities the logarithm of the saturated rock conductivity is directly proportional to the logarithm of the electrolyte conductivity – this is the region of bulk conductivity. At low electrolyte conductivities this relation is no longer valid: the saturated rock conductivity tends to a constant value representing surface conductivity (Figure 12). The interpretation of the Cole–Cole diagrams for these data indicated that Na^+ ions were adsorbed on quartz grain surfaces.

Wildenschild et al. (2000) studied such phenomena in more detail when measuring the electrical response at a fixed frequency of 1 kHz on different

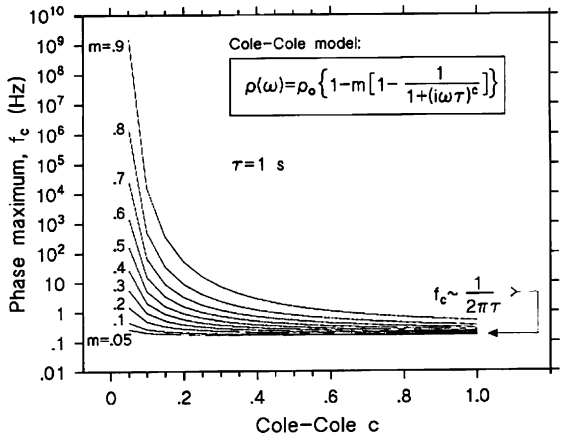

Figure 10. Experimental points and fitted theoretical curves for the effective normalised conductivity σ/σ_w variation with normalised frequency on a logarithmic scale (Vanhala, 1997).

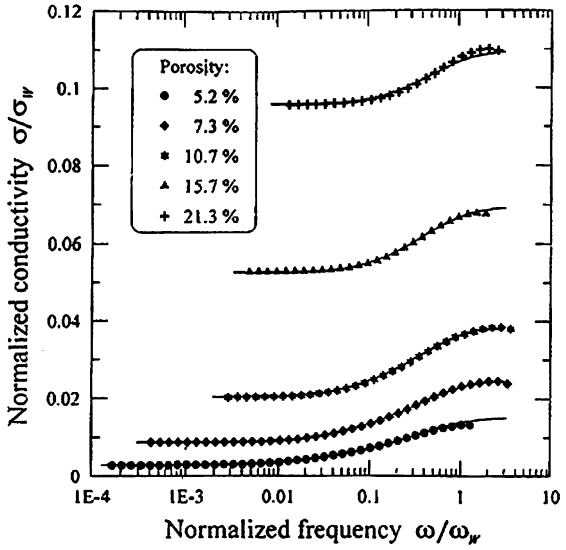

Figure 11. Electrical conductivity of samples of Berea and Darley Dale sandstone saturated with NaCl solutions of various concentrations as a function of the electrical conductivity of the electrolyte solutions: Triangles – Berea; circles – Darley Dale (Haslund and Nost, 1998).

sand–clay mixtures. Variables in the measurements were the clay content that was increased from zero up to 10% montmorillonite and the packing geometries that were set to dispersed, clusters and parallel layering. Using these boundary conditions they distinguished between the bulk conductivity (σ_{bulk}) in the electrolyte and surface conductivity. Electrolyte conductivities (σ_{fluid}) were varied from 10^{-4} up to 6.4 S/m using distilled water and $CaCl_2$ solutions

of up to 0.75 N. The results confirmed that the surface conductivity dominates the charge transport in dilute electrolytes. Two different regions are visible in Figure 13, at high fluid concentrations(> 1 S/m), σ_{bulk} has a power-law dependence on σ_{fluid}, and the gradient of the line is approximately unity. Movement of ions through the bulk fluid is the dominant conduction mechanism. However, at low fluid concentrations (< 1 S/m), σ_{bulk} is no longer solely dependent on σ_{fluid}. In this region, surface conductance due to mobile ions in the electrical DL becomes more important; the curves tend to a constant, which represents surface conductivity (Revil et al., 1998).

A linear dependence between bulk conductivity and fluid conductivity was measured when salt concentrations were above the threshold value. An increase of the clay content from 3 to 10% shifts the intercept to higher values of surface conductivity from 0.018 to 0.0576 S/m, whereas clean sand exhibits the lowest value, 0.0054 S/m (Figure 13). The configurations of the clays are also of importance for the measured conductivities. Clustered clay exhibits the lowest values whereas parallel configurations produce the highest surface conductivity values. The intercept with the ordinate axis of Figure 13 defines a parameter b that can be used to calculate surface conductivity from the known formation factor F, the intercept b and Λ considering the geometry of the porous medium (Carman, 1965; Revil et al., 1996).

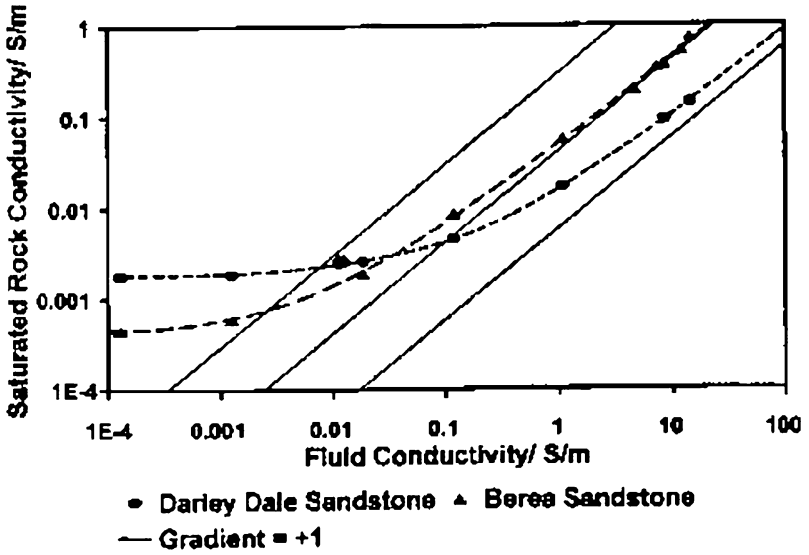

Figure 12. Log–log plot of bulk conductivity versus fluid conductivity for various mixtures and distributions. For σ_{fluid} below 0.2 S/m the surface conductivity becomes a dominant factor in the total conductivity. Above this value the bulk conductivity is relatively sensitive to clay content and distribution (Glover et al., 1994).

$$\Sigma_s = b\Lambda F/2 \quad \text{and} \quad \Lambda \approx V_p/S \tag{23}$$

where V_p is pore volume and S the inner surface area of the pore system. Similar results were reported by Johnson and Manning (1986), Sen (1984) and Revil et al. (1998). Their results show the significant influence of surface conductivity on bulk electrical properties, especially for porous samples saturated with dilute electrolytes and low porous low permeable samples where the thickness of the DL is the same order as crack width.

Roberts (2002) performed conductivity measurements on porous tuffs in the temperature range of 23 to 145 °C. Porosities ranged from 0.089 to 0.135, and saturation conditions were set from 20 up to 100%. An Arrhenius behaviour of the conductivity was detected in the temperature range up to 145 °C. Activation energies E_a (using $\sigma = \sigma_o \exp(-E_a/kT)$) were found to be negatively correlated with saturation, and decreased with increasing saturation from 0.28 down to 0.15 eV (Figure 14). The times required for equilibrium of conductivity are rather short. After a step change in pore pressure it is about 10% of the time for the pressure pulse. If samples were partially saturated and pore pressures were high due to a temperature increase, the conductivity was

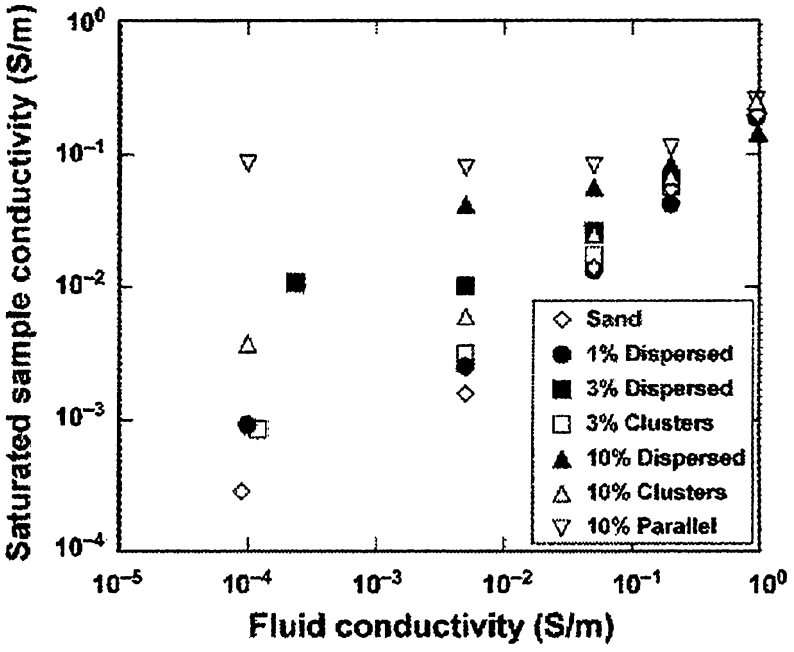

Figure 13. Log–log plot of bulk conductivity vs. fluid conductivity for different sand-clay mixtures and distributions. For fluid conductivities below about 0.2 S/m surface conductivity becomes a dominant factor in the total conductivity (Wildenschild et al., 2000).

found to be comparable with that of 100% saturation. But if pore pressure were lowered below the boiling point a decrease of the conductivity was measured. At low saturation conditions, $< 20\%$, Roberts et al. (2001) report an exponential dependency of the resistivity

$$\rho = \rho \exp(CS_{\mathrm{w}}) \tag{24}$$

where C is a constant and S_{w} is the saturation. This equation provides the best match with the laboratory data for all temperatures and saturations. A mixed conduction process of bulk and surface conductivity is most likely at low saturation conditions. A surprising result was that a large volume of pores will stay filled with liquid even at relatively low pore pressures. This has implications for, e.g., reservoir engineering, radioactive waste disposal and exploration techniques.

El-Kaliouby et al. (2001) measured the polarisability of a water saturated sand–clay–hematite mixture in the frequency range from 1 Hz up to 100 MHz. They tested the validity of a Cole–Cole model in the frequency range from 5 Hz up to 500 kHz which is of interest for correlation with transient electromagnetic measurements (TEM) performed in the time domain. Forward modelling and neural network inversion were used to derive the essential Cole–Cole parameters of chargeability m, the time constant τ and the frequency parameter c:

$$\sigma(\omega) = \sigma_{\mathrm{o}}[1 + (\mathrm{i}\omega\tau)^c]/[1 + \alpha(\mathrm{i}\omega\tau)^c] \tag{25}$$

where σ is the conductivity, $\alpha = 1 - m$ and $\mathrm{i} = \sqrt{-1}$. Dispersion was detected in the measured data in the low frequency range due to membrane polarisation caused by the clay content. The high frequency response is due to the bulk properties of the constituents. To fit the measured data, a two-layer model with an upper polarisable layer and a three layer model including a second polarisable layer were used. Forward modelling with an upper, partially saturated aquifer showed that such a layer has a negligible effect on the response.

4.1.2. *Pressure dependence of the conductivity*

A theory explaining the influence of pressure on the electrical conductivity was published by Johnson and Manning (1986). Fracture closing due to applied confining pressures was modelled on the basis of percolation theory using an isotropic network of pores and cracks that closed randomly. They were able to explain why fractures with a high aspect ratio are closed first at low confining pressures, while at higher pressures the intrinsic properties of

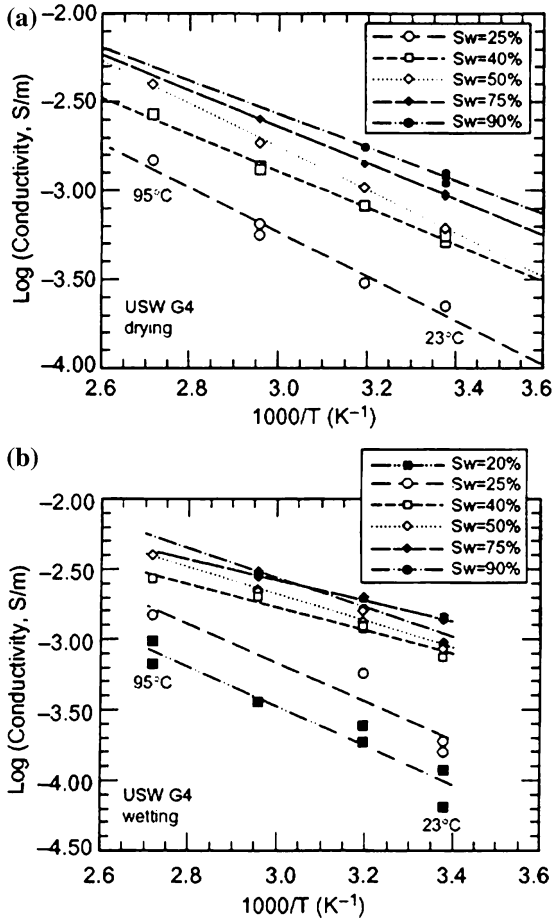

Figure 14. Log conductivity versus reciprocal temperature for a tuff sample between 23 and 95 °C, for both wetting (a) and drying (b) at varying saturations. Straight line fits using an Arrhenius relationship are shown. Activation energies range between 0.15 and 0.28 eV (Roberts, 2002).

the pores dominate the decrease of pore volume. This was confirmed by various groups that measured decreasing rock conductivity when hydrostatic pressures (uniaxial and confining (mantle) pressures are equal) were applied. Measurements were performed on sedimentary and crystalline rocks. These experiments were not only a simple confirmation of theoretical considerations but aimed on a better understanding of, e.g.,

(i) the electrical signature of fracture closing (Moret and Le Mouel, 1987, 1992; Shankland et al., 1997; Fowler et al., 2005; Freund and Nover 1995; Nover et al. 2000, 2001, 2005),
(ii) the opening of fractures in reversed (stress) experiments (Heikamp and Nover, 2003),

(iii) surface conductivity (Nover and Stoll 2005),
(iv) reconnection of highly conducting phases when fractures close (Glover and Vine, 1992; Duba et al., 1994; Fowler et al., 2004; Nover and Stoll, 2005).

The last aspect may be used to explain highly conductive zones in the Earth's crust (Section 4.2.1).

Heikamp and Nover (2003) measured pressure-induced variations in pore geometry on dry and fluid saturated low porous (< 0.02) low permeable (< 5 nD) marble samples. Hydrostatic and uniaxial pressures were applied. Pressure-induced closing of open fractures and a reduction of the aspect ratio caused an increase of the bulk conductivity in hydrostatic pressure experiments (Figure 15). In contrast to this an increase in conductivity was measured when uniaxial pressures were applied. The opening of new cracks increased the conductivity and thus increased the inner surface of the pore system. This increase in pore surface corresponds with an increase of the surface sensitive model capacitor that was derived from a least squares refinement of the frequency dependent complex conductivity data. The increase of the value of the capacitor was moderate when stress conditions were not close to the stability limit of the sample, but before failure a sharp increase indicates clustering of new fractures. The value of the capacitor was decreased in hydrostatic pressure experiments.

The pressure dependence of the complex electrical resistivity of porous sandstones from gas drillings was measured by (Duba et al. 2001; Nover et al. 2004a, 2004b). They used frequency dispersion data in the frequency range 800 Hz up to 1 MHz to explain surface conductivity and to present a qualitative permeability–conductivity relation. The complex response was interpreted using an equivalent circuit model consisting of two RC-elements in series. Resistor R2 increases as a function of pressure, reflecting the closing of fractures and the decrease in connectivity of the pore system. The reduction of the inner surface area was detected in C2 that exhibited a decrease by about half an order of magnitude. The model capacitor C2 showed a lithology effect (anisotropy) being different for one sample when measured in the foliation (X, Y) and perpendicular to it. A crossplot of the presure dependence of C2 versus the pressure dependence of the permeability resulted in a straight line (Figure 16). The slope of the lines of various samples and spatial orientation reflected the lithology and were indirect measures for pressure-induced variations in the inner surface area.

4.2. Electronic conduction

Carbon is one possible candidate for causing high conductivity anomalies of the Earth's crust. Using the upper bound formula, Duba and Shankland

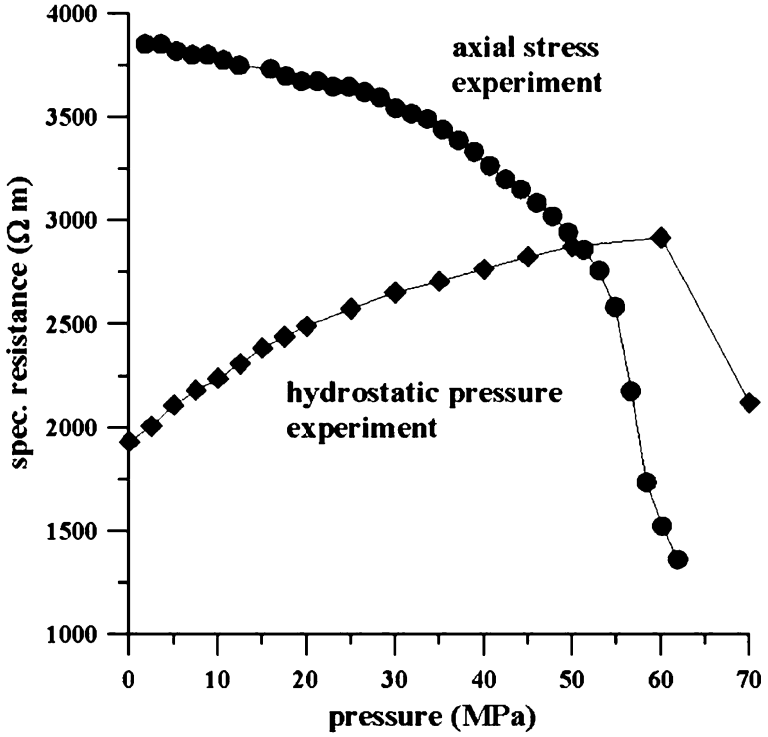

Figure 15. Response of the bulk resistance of a limestone sample saturated with a NaCl solution of 0.1 molarity in a hydrostatic and a uniaxial loading pressure experiment. Due to the closure of open fractures the resistance was increased in the hydrostatic experiment, whereas a continuous decrease of the bulk resistivity was observed in the uniaxial loading experiment (Heikamp and Nover, 2003).

(1982) calculated the absolute amount of highly conductive and well-interconnected carbon required, and found that a volume fraction of only 5×10^{-6} vol% of carbon was necessary to enhance the electrical conductivity of dry rocks to values typical for conductive zones at lower crustal conditions (0.1 S/m). Highly conducting zones can thus be explained in principle by metallic conduction in graphite if the carbon layers are well interconnected. In view of the tectonic history of rocks, convincing models for the transport and deposition of carbon, either as organic matter or in the gas-phase, are required.

4.2.1. *High electrical conductivity caused by graphite*

Carbon-enhanced conductivites of crustal rocks were reported by Glover and Vine (1992), who measured electrical conductivities at fixed frequencies on fluid saturated graphite free and graphite-bearing crystalline rocks (Figure 17). The samples were exposed to increasing pressures and tempera-

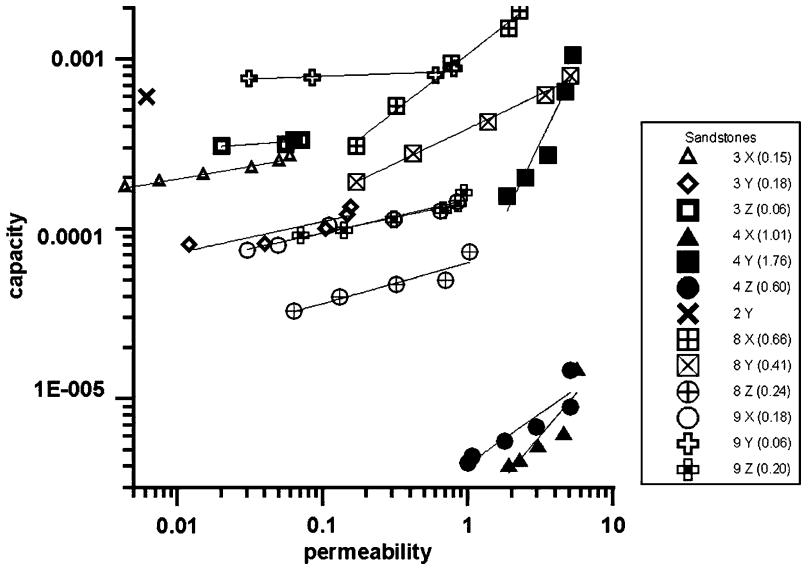

Figure 16. This diagram displays a cross-correlation of the pressure dependence of the permeability and of an electrical parameter that was derived from a least-squares refinement of model data that were fitted to the measured frequency of the complex electrical response. The numbers (2, 3, 4, 8 and 9) are for the different samples, X, Y and Z stand for the orientation of the sample in regard to foliation and lineation; X is the direction of the lineation, X–Y is the foliation plane, and Z is perpendicular to the foliation plane. The abscissa shows the permeability, while the ordinate displays a complex quantity, a refined model capacitor; this measure can be related to the inner surface of the pore system. The lines between the points are simply a guide for the eye; they show in which way permeability and electrical properties change as a function of pressure. Pressure increases along the lines from right to left. Identical samples, but different in orientation in regard to the texture exhibit different pressure dependencies of permeability and electrical properties. These data will be used for a better permeability–conductivity relation.

tures (0.2 GPa, 900 °C), thus establishing the *in-situ* p,T conditions of a lower crustal environment. The results showed that increasing the pressure decreased the bulk conductivity in the graphite free samples caused by a reduction of the pore fraction where 'electrolytic' conductivity could take place. This decrease in conductivity is typical of graphite free samples, but was reversed when graphite-bearing granulites were measured. In this case the samples exhibited an increase in conductivity though fractures were closed and electrolytes were squeezed out of the pores. These results were confirmed on graphite-bearing granulites measured both dry and fully saturated. In both cases the conductivity increased when pressure was applied and the fractures closed.

Cores samples from the German Continental Deep-Drilling Program (KTB) revealed interconnected conductive graphitic veins and shear zones as well as disconnected, isolated graphite crystals (Zulauf, 1992; Kontny et al.,

1997). In cataclastic fault zones, graphite is associated with mineral assemblages suggesting deposition temperatures of 250°to 340 °C and pressures < 200 MPa. This graphite extends over distances of at least some kilometres as proved by plug-, borehole- and field-measurements (ELEKTB, 1997; Stoll et al., 1992, 1995, 2000). Mogk and Mathez (2000) report that at a depth of 9.1 km the carbonaceous material is predominantly elementary carbon. At a shallower depth of about 4.6 km a mixture of elementary carbon, simple hydrocarbons (such as alkanes and possibly C–O–H compounds) were detected using time of flight secondary ion spectroscopy (TOF-SIMS) and electron probe analysis. Carbonaceous matter and retrograde formed minerals on microcracks were formed together at high crustal levels and much later than peak metomorphism. Due to the production of hydrocarbons during retrograde metamorphism grain boundary and microcrack carbon was mobilised, and thus the degree of interconnection of the carbon network was reduced.

Shankland et al. (1997) measured an unusual pressure effect on graphite-bearing fluid saturated KTB core samples. Increasing the confining pressures caused an increase in conductivity due to a higher degree of reconnection of graphite on open fractures of the samples. Using percolation theory and the slope of the pressure versus conductivity curve, Shankland et al. (1994) calculated the fraction of reconnected carbon bonds when pressure was applied. A minimum value of 25% for the degree of interconnection p_c is required to form a three-dimensional network.

This finding was verified by Nover et al. (1998) who studied the complex conductivity on 8 KTB core samples from a micro-profile of the drilling. In this cataclastic section (7012 m in depth), higher concentrations of graphitic carbon on fractures were detected in the amphibolites. Seven of the samples exhibited a normal pressure – conductivity dependence, though the conductivities of all samples were enhanced by at least two orders in magnitude in comparison with graphite-free samples. When pressure was raised up to 200 MPa an increase of the conductivity by about a factor of 1.4 was detected. The conductivity was further increased (by a factor of 1.8) when the sample was kept at 200 MPa for more than 600 h. The complex response showed 'quasimetallic' charge transport through the reconnected graphite network as a function of time, whereaselectrolytic conduction diminished.

Jödicke et al. (2004) reported graphite (3% by volume) enhanced conductivity in metapelites from Calabria. A high conductivity of up to 50 S/m was detected in some sequences of the metapelites where an interconnected network of iron sulphides and graphite was formed on shear planes. In the highly conducting samples the frequency dependence was measured in the frequency range 10^{-3} to 10^{5} Hz. No significant changes in the absolute values of the conductivity and phase angle were detected as a function of frequency, indicating 'quasimetallic' conduction through the interconnected network of

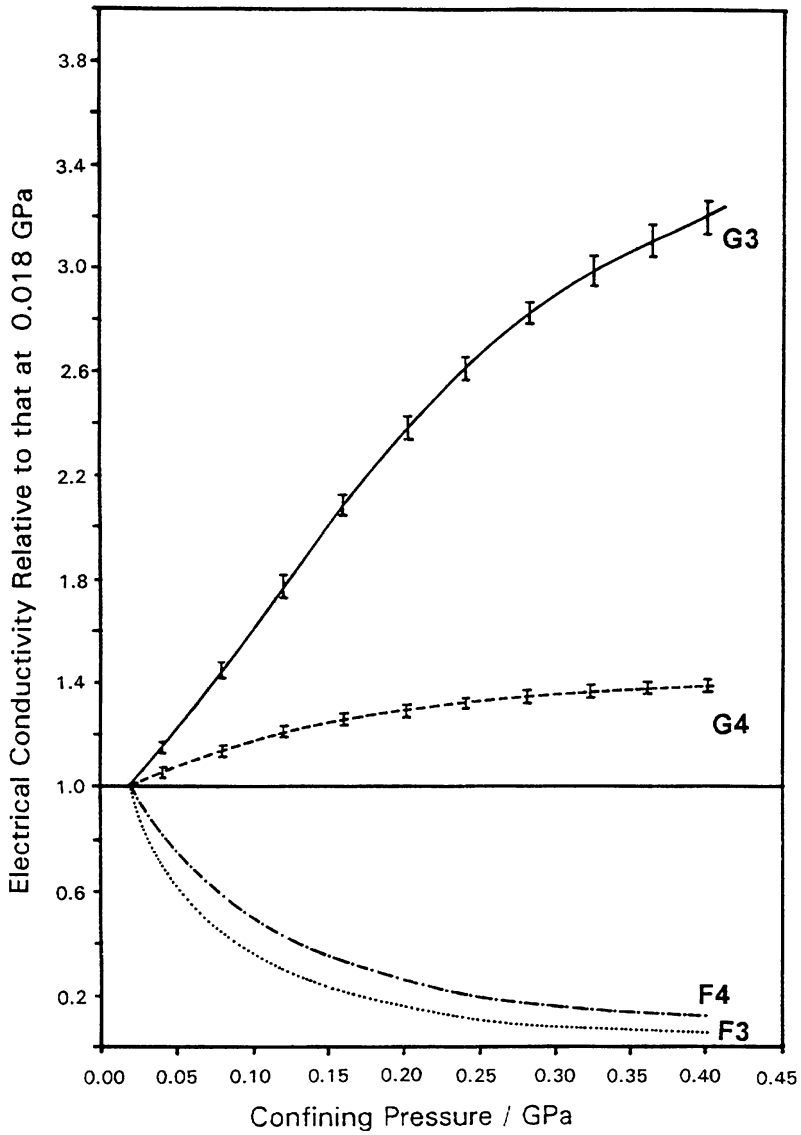

Figure 17. The variation of the electrical conductivity of unsaturated samples of carbon free (F3/F4) and carbon-bearing (G3/G4) granulites when subjected to raised confining pressures. G3/G4 measurement direction parallel and perpendicular to carbon foliation; F3/F4 no foliation. Data are normalised to values at 18 GPa (Glover and Vine, 1992).

carbon. This was confirmed by measurement under dry and fully saturated conditions. For comparison, additional carbon-bearing metapelites (3% by volume) from other locations were studied, but in these samples all of the carbon was concentrated in the form of isolated grains. The conductivity of these samples was not enhanced above the value typical for such rocks.

Hoffmann et al. (2001) interpreted deep-seated good conductors in the North German Basin considering highly conductive black shales to be the cause. To prove this they measured the complex conductivity on black shale rich core samples from the Münsterland drilling and found a perfect frequency independence, together with high conductivities in the frequency range from 10^{-3} to 10^{6} Hz. Phase angles were close to 0°. Consequently metallic conduction dominates the charge transport in the carbon rich rocks (5–8%) of the meta-anthracite stage. A discontinuity in the conductivity profile of the Münsterland drilling borehole was detected at the boundary of the meta-anthracite stage. Hoffman et al. (2001) deduced that, at this depth, the transition from less ordered, poorly conducting carbon to well-ordered graphitic carbon occurs. The observed vitrinite reflectance supports this.

The electrical conductivity of high schistosity black shales from bore holes in Vernier, Switzerland, was measured by Losito et al. (2001). The samples were studied under simulated environmental conditions at temperatures of up to 180 °C, confining pressures of 39 MPa and a pore pressure of 23 MPa. Complex data were measured in the frequency range from 0.005 to 200 Hz using 2- and 4-electrode techniques on samples oriented parallel and perpendicular to the layering of these carbon-bearing shales. They found a significant anisotropy in conductivity (about one order of magnitude) but measured a normal pressure effect when confining pressures were increased and fractures closed. An unusual pressure effect was detected on those samples where a reconnection of the conductive carbon network was observed when confining pressures were increased and fractures closed.

Monteiro Santos et al. (2002) interpreted deep-seated crustal anomalies in SW Iberia by using a modified brick-layer model. They calculated the graphite fraction required to cause high electrical conductivity. This modified model allowed the conductivity enhancement to be calculated due tointerconnected graphite films:

$$\sigma = (\sigma_1(f^{2/3} - 1) - \sigma f^{2/3})/(\sigma_s(f - f^{2/3}) + \sigma_1(f^{2/3} - f - 1)) \tag{26}$$

where σ is the resulting conductivity, σ_1 the conductivity of graphite, σ_s the conductivity of grains and $f = 1 - x$, where x represents the volume fraction of the graphite. The calculations suggest that a fraction below 0.02% of graphite is sufficient to explain the measured conductivities.

Carbon enhanced conductivity was detected by Fowler et al. (2004) on carbon-bearing and carbon-free drill cores from the Trans Hudson Orogen. In the complex impedance spectra, carbon rich samples (1 to 10% carbon plus up to 10% ores; porosity $< 1\%$) exhibited a Cole–Cole response typical for electrolytic conduction. They assumed that a low degree of interconnection of the highly conducting phases was present. In contrast to this,

well-interconnected graphite was detected in one of the samples, though the absolute amount of carbon was only in the range of 3%. The corresponding Cole–Cole diagram exhibited the typical response for metallic conduction by a negligible contribution of the imaginary part of the conductivity and no frequency dependence (1 kHz to 1 MHz) of complex quantities (Figure 18). This finding was supported by time dependent measurements performed at elevated pressures. Though fractures were closed, and the contribution of electrolytic conduction to the total conductivity was reduced, the frequency dependence of the conductivity decreased.

4.2.2. *Graphitisation of less ordered carbon*

Graphitisation is the final stage of a maturation process by which organic matter loses adsorbed volatiles. This loss of mobile phases (H_2O, CH_4, N_2, etc.) is a purification process that will finally result in chemically pure carbon but with a low degree of ordering of the hexagonal carbon rings. As graphite is often found in metamorphic rocks with a certain tectonic history the influence of such parameters on graphitisation of less ordered carbon was studied by various groups (Rouzaud et al. 1990; Ross et al. 1990). From technical processes it is well known that graphitisation requires temperatures > 2000 °C if no pressure or stress is applied, but such high temperatures are unrealistic for natural processes. In nature graphite is found in different stages of ordering in green schist metamorphism, that means at temperatures lower than 700 °C and pressures below 0.6 GPa. Graphitisation is an ordering process beyond the anthracite stage of the coalification process.

4.2.2.1. *Coalification*. In meta-sedimentary strata carbon is generally assumed to originate from progressive metamorphism of kerogen under low pressure and temperature conditions. This biogenic process of coalification of organic material from peat to anthracite is a maturation process where organic material loses adsorbed volatiles. The purity of the carbon-phase increases from approximately 60–70% C for peat up to 90–97% C for anthracite. At the same time the degree of molecular ordering and of interconnection of the carbon-sheets is increased. Temperature accelerates the chemical reactions during coalification, whereas pressure promotes a physico-structural organisation of the carbon network (Teichmüller and Teichmüller, 1982).

4.2.2.2. *Graphitisation*. The next step is the transformation of less-ordered carbon into well-ordered graphite. This process is not understood in detail, but petrological findings show that natural graphite is formed at temperatures as low as 300–500 °C and pressures of 0.4–0.5 GPa. This means that graphitisation takes place for upper green schist metamorphic conditions. Beside the environmental p,T conditions, tectonic movement and the reaction

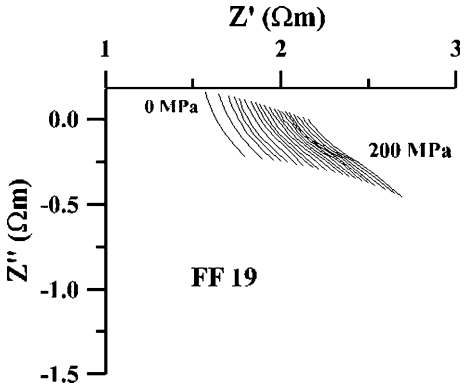

Figure 18. Cole–Cole diagram of the complex response of the 10% carbon-bearing sample FF19. Data points are close to the real axis, thus indicating electronic conduction. Note the different scales on the *X* and *Y* axes (Fowler et al., 2004).

time have a significant influence on the quality of graphite in a crystallographic sense. The graphitisation of coal required much higher pressure and temperature conditions. Bituminous coal ('hard' coal) requires temperatures of around 2200 °C if no pressure is applied; lignite or sub-bituminous coal do not show graphitisation even at temperatures of up to 3000 °C (Oberlin, 1984). Consequently, temperature alone could not be the only driving force causing graphitisation of organic matter (Bonijoly et al., 1982).

Fonton et al. (1980) found that graphitisation develops discontinuously with sudden improvements in the degree of molecular ordering. The turbostratic (amorphous) structure of anthracite disappears by partial graphitisation. This first step of graphitisation requires high temperatures and pressures, and is enhanced by shearing and stretching. Finally, true graphite is formed as a three-dimensional arrangement of the layers is attained, combined with the rapid increase of layer diameter to 5 mm or more.

Wilks et al. (1993) reported a reduction of the required transformation pressure and temperature when shear stress was applied (900 °C, 1.0 GPa). An enhanced ordering of the graphite crystallinity was detected by an increase of the (002) graphite reflection intensity. This finding was improved by transmission electron microscopy (TEM) of tectonically deformed anthracite showing that, along with temperature, stress/pressure is required to align the 'aromatic' lamella.

Nover and Stoll (2005) studied the kinetics of graphitisation using electrical conductivity data and energy dispersive X-ray diffraction. The experiments were performed under green schist facies conditions. The frequency dependence of the conductivity was measured in the frequency range of 1 to 100 kHz. Two kinds of experiments were performed. In 'shear' experiments a differential stress acted on the sample. This was generated by a modified

setup of the reaction cell. In 'strain' experiments the upper and lower pistons were inclined by a about 30°, thus causing a strain rate of about 6×10^{-7} s^{-1}. In both experiments an increase of bulk conductivity was measured as a function of time. This increase was more pronounced in the strain experiment. At the same time a decrease of the imaginary part of the impedance was detected this means that metallic charge transport dominates after long-reaction times (up to 4 weeks). This finding, together with the energy dispersive X-ray diffraction detection of structural changes, confirmed that pressure, shear and temperatures as low as 300–500 °C were sufficient to transform good quality coal into well-ordered graphite. In these experiments graphitisation of organic material was reproduced in the laboratory under upper green schist facies conditions.

4.2.2.3. *Abionic graphite precipitation*. Besides the biogenic graphite formation, abionic graphite precipitation is often discussed as a possible process for carbon transport and, subsequently, the reduction or oxidation of the carbon-rich fluid phases like CO_2 and CH_4. In a formal chemical reaction Walther and Althaus (1993) described the graphite precipitation as $CO_2 + CH_4 \rightarrow 2C + 2H_2O$ without saying by which process the required activation energy is supplied to reduce or oxidise the gases. Thus the principal features of abionic graphite precipitation are not known. On the other fluid inclusion studies on graphite-bearing amphibolites from the KTB borehole show the coexistence of N_2, CH_4 and CO_2. Highly crystalline graphite was found in thin films on shear planes. Walther and Althaus (1993) concluded that graphite was precipitated from a methane-carbon dioxide fluid. They suggest that the activation energy for the reduction of CO_2 and the oxidation of CH_4 should be provided by heat generation during tectonic movement (a mechanical–tribochemical mechanism).

Roberts et al. (2001) simulated these chemical and physical boundary conditions in a sophisticated experimental setup. They measured in an internally heated gas-pressure vessel changes of electrical conductivity on the Nugget sandstone and Westerly granite during rock fracture in a carbonaceous gas-atmosphere. Samples were deformed and fractured at temperatures between 354 and 502 °C, while the pressure was set to 100 and 170 MPa. An increase in conductivity was measured under *in-situ* conditions during dilatancy and fracturing. They found that the reactive, newly formed surfaces provided the required activation energy for the reduction or oxidation of the CO_2 or CH_4 gas phases. The increase in conductivity could be due to carbon deposited and interconnected by this process onto the fresh surfaces (Figure 19). TOF-SIMS allowed the distribution of carbon in the sample to be measured. Mapping exhibited the presence of carbon on microcracks that were assumed to have formed during fracturing. This finding led to the

hypothesis that carbon is deposited as a continuous film on the new, reactive mineral surface formed during microfracturing.

The crucial points (origin, mobility, precipitation and interconnection) lead to an understanding of the role of carbon in enhanced crustal conductivities. Different models for the explanation of carbon mobility (mobilisation) have been presented, but (due to thermodynamic considerations) arguments for carbon transport via the gas phase and subsequently via precipitation are not yet conclusive. An important question is how interconnected graphite films can extend over distances of several kilometres in view of crustal tectonics and dynamics.

4.3. Temperature-induced semiconduction

The Earth's mantle shows significant electrical anomalies at depths ranging from 400 down to 670 km. These discontinuities were detected by MT soundings (Figure 20) and resulted in a conductivity jump of up to or even more than 1.5 orders of magnitude depending on the model used. From phase stability considerations it was suggested that the conductivity jump should be caused by the $\alpha \rightarrow \beta \rightarrow \gamma$ phase transition in olivine. This phase transition changes the density and the crystallographic structure of $(Mg,Fe)_2SiO_4$ from orthorhombic to cubic symmetry, that means the transition from the olivine into the spinel phase. From laboratory conductivity measurements on the olivine and spinel phase it is known that the conductivity of spinel is enhanced in comparison with the olivine phase due to the atomic arrangement of oxygen, silicon magnesium and iron in the basic structural unit. Reliable data on the magnitude of the conductivity jump are not yet available. This is mainly due to experimental problems when measuring conductivity data under *in-situ* p,T conditions required for the $\alpha \rightarrow \beta \rightarrow \gamma$ phase transition in laboratory experiments. The pressure required are more than 14–16 GPa and the temperatures have to exceed 1400 °C. As we now know, the kinetics of the transition require reaction times for each change in temperature and pressure from some hours at high p,T conditions to some days at temperatures below 900 °C in order to reach stationary conditions in the conductivity record (Nover et al., 1992; von der Gönna, 1997). To solve this problem three different approaches were tested.

(1) The principles of the electrical charge transport were investigated on natural and synthetic olivines having different fayalite content at pressures of up to 2 GPa and temperatures of up to 1600 °C (Duba et al., 1973, 1974, 1982, 1993; Hinze et al., 1981, 1982; Manko 1984; Cemic et al., 1978, 1980; Schock et al., 1989; Shankland et al., 1974, 1979, 1997). The main aim was to study the influence of temperature, pressure and

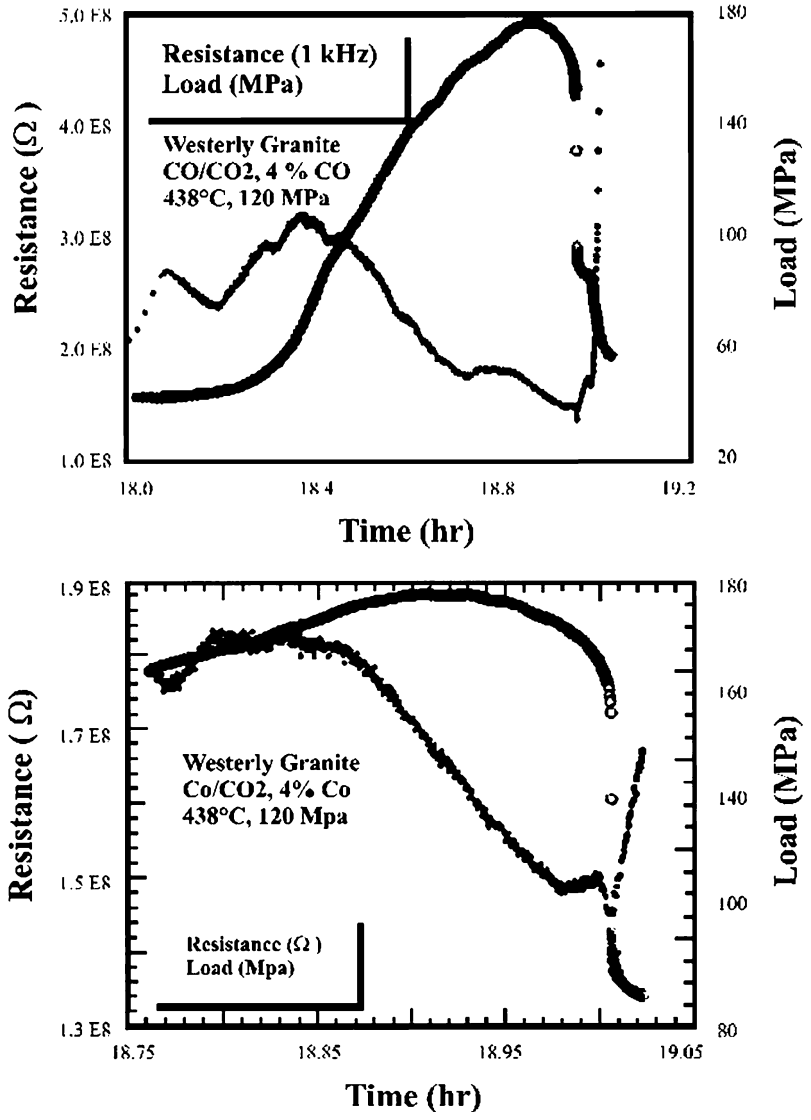

Figure 19. Electrical resistance (solid circles) and load (open circles) as a function of time of Westerly granite. The sample was run at 438 °C in a CO–CO_2 atmosphere. (a) The entire loading cycle. (b) Detail during the main fracture event. Resistance generally decreased during the loading cycle as dilation occurred. Small increases in resistance near 18.74 and 18.96 h indicate that conductive paths are continually being formed and broken (Roberts et al., 1999).

thermodynamic conditions (such as oxygen fugacity) on the electrical charge transport. Subtopics are:

(1.1) temperature-induced semiconduction (kinetics, times required for stationary conditions) and influence of thermodynamic parameters on conductivity and charge transport (pressure temperature and

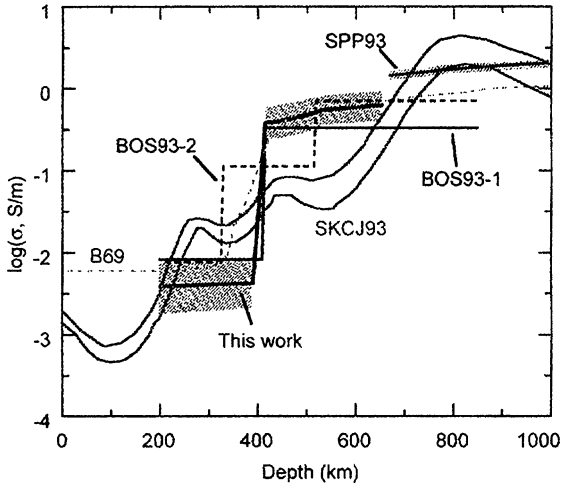

Figure 20. The conductivity model for the upper mantle calculated from laboratory data (thick black line) with the addition of a lower mantle curve for perowskite + magnesiowüstite having a bulk iron fraction Fe/(Fe + Mg) = 0.11. Shaded areas illustrate the effect on the model of a ± 100 °C temperature variation. Geophysical models are shown as B69, BOS93-1 BOS93-2 and SKCJ93. The estimated uncertainty in the laboratory based models is ±0.3 log units (Xu et al., 1998).

oxygen fugacity; iron-bearing olivines require oxygen fugacity control because of its influence on the oxidation state of iron, being Fe^{2+} under reducing or Fe^{3+} under oxidising conditions, respectively)
(1.2) charge transport process (mobility of the different species of possible charge carriers)
(1.3) directional dependence of conductivity (single crystals).

(2) A second approach focussed on a structural homologue phase, magnesium-germanate (Mg_2GeO_4) (Nover et al., 1992, von der Gönna, 1997). This phase requires much lower pressures (only 2 GPa) for the $\alpha \rightarrow \beta \rightarrow \gamma$ transition. Consequently, the temperature dependence of the conductivity and the kinetics of the phase transition could be studied under well defined thermodynamic conditions in conventional high-pressure devices. In parallel to the electrical measurements X-ray diffraction techniques could be used to have more information on the kinetics of the transition. The low transformation pressure of the germanate is caused by the larger ionic radius of Ge^{4+} (0.053 nm) than of Si^{4+} (0.042 nm).

(3) Finally, when sophisticated HPHT devices like multi-anvil cells could be used, the p,T range required for the transition was accessible. However, due to the design of the pressure cell, long time high temperature measurements were not possible due to ineffective cooling of the whole device. Consequently, the electrical data reported on the $\alpha \rightarrow \beta \rightarrow \gamma$

transition were measured far beyond any thermodynamic stability and thus have to be handled with caution. Subtopics are:

(3) (3.1) The phase transition olivine into spinel causes silicon to be in 6-fold coordination instead of 4-fold in olivine. This increases the density and decreases the volume of the elementary cell by about 8%. As the nucleation of spinel starts from olivine grain boundaries, the kinetics of the transformation are directly affected due to the pressure release. This has consequences on the larger scale for the electrical properties of a subducting slab, as well as for the transformation on the laboratory scale.

If the transport process of the charge carriers in the α,β and γ phase is well understood, then these data can be used for a interpretation of conductivity changes in the Earth mantle. Conductivity measurements were performed on both synthetic and natural samples, the end members forsterite and fayalite, as well as San Carlos olivine, Red Sea Peridotite and Dreiser Weiher olivine (Duba et al., 1973, 1974, 1982, 1993; Hinze et al., 1981, 1982; Manko 1984; Cemic et al., 1978, 1980; Schock et al., 1989; Shankland et al., 1974, 1979, 1997). From (1) it is known that the electrical conductivity of olivine depends on the defect concentration and mobility of possible charge carriers. This means that variations in the point defect structure of olivine (in the pressure and temperature range of upper/lower mantle conditions) controls the electrical charge transport. The significant influence of these parameters on measured conductivity data are displayed in Figures 21 and 22. Both figures show in an Arrhenius diagram (reciprocal temperature vs. log conductivity) the influence of various oxygen partial pressures on the electrical conductivity. Different buffer mixtures within the stability field of olivine were used define the oxygen partial pressure (from reducing to oxidising atmosphere: FQI – fayalite–quartz-iron; IW – iron–wüstite; G – graphite; WM – wüstite–magnetite; FQM – fayalite–quartz–magnetite. Fayalite is much more conductive than forsterite, due to its iron content, whereas in forsterite the defect stoichiometry controls the conductivity.

The first experimental data on the conductivity of olivine were published by Duba and Nicholls (1973) and Duba et al. (1974). Since that time a large number of conductivity measurements were performed, but the data did not seem to be reproducible due to different experimental setups, controlled or uncontrolled oxygen fugacity and the various frequencies at which conductivity measured (from DC up to some kHz). Experimental setups today are much more complicated; besides precise pressure and temperature control well defined oxygen fugacities can be applied (Cemic et al., 1978, 1980; Hinze et al., 1981, 1982; Schock et al., 1989; Constable and Duba, 1990; Constable et al., 1992). Oxygen partial pressures can be varied within the stability field of olivine, and measurement of the frequency dependence of the complex electrical conductivity is also possible. Frequency dispersion measurements pro-

vide further information on the charge transport (Manko, 1984; Nover et al., 1992; Roberts and Tyburczy, 1993; Constable and Roberts, 1997; Xu et al., 1998, 1999, 2000). Activation energies reported today on olivine, forsterite and fayalite are much more homogeneous due to the control of the thermodynamic environment in the experiments.

But time is still a limiting factor for the quality of the measured data. Most of the variations in reported conductivity data are due nucleation, recrystallisation, growth of the grains and grain-coarsening; the electrical conductivity is very sensitive to these parameters. In an experiment stationary conditions are essential, especially when powder samples are used. The stability considerations are the reason why recently reported conductivity shifts on the $\alpha \rightarrow \gamma$ transition for olivine should be handled with caution. Most of these experiments were performed rather quickly without any control of stationary conditions due to the experimental difficulties mentioned above (Akimoto and Fujisawa, 1965; Omura, 1991; Duba and von der Gönna, 1994; Xu et al., 1998).

4.3.1. *Electrical charge transport in olivine*

Duba and Nicholls (1973) measured the electrical conductivity of the San Carlos Olivine in the [0 0 1] direction, as a function of temperature and oxygen fugacity pO_2, to prove that the conductivity of olivine was controlled

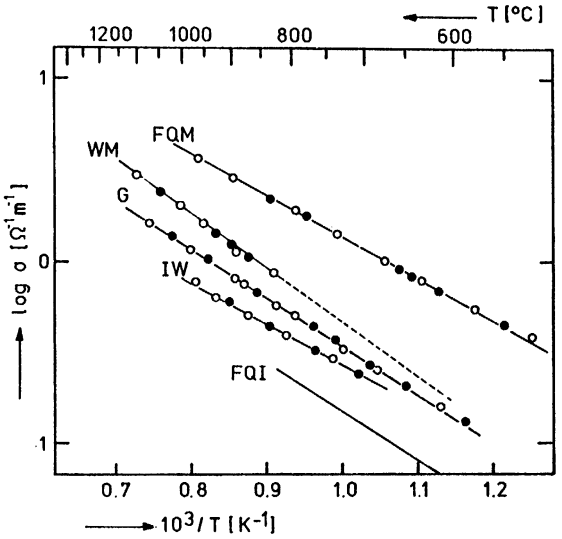

Figure 21. Arrhenius diagram of the conductivity of fayalite at various oxygen partial pressures in the stability field of olivine. Reducing conditions are given by the buffer mixture FQI-fayalite quartz iron, whereas oxidising conditions were established using a fayalite quartz magnetite (FQM) buffer mixture. WM – wüstite magnetite; G – graphite; IW – iron wüstite (von der Gönna, 1997).

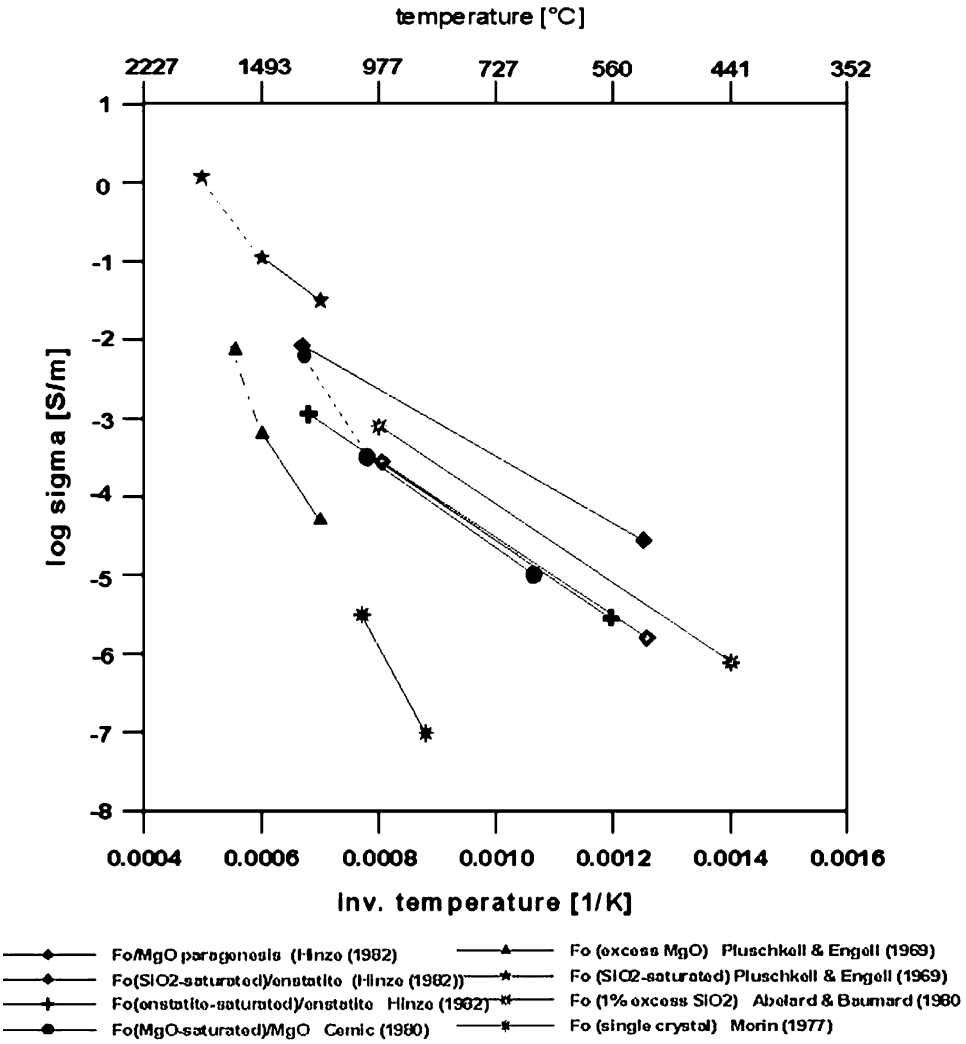

Figure 22. Arrhenius diagram of the conductivity of forsterite at various oxygen fugacity conditions. The buffer mixtures used are shown at the bottom of the diagram (von der Gönna, 1997).

by the oxidation state of iron. Heating of the sample enhanced the conductivity as a function of temperature, but a subsequent variation of the oxygen fugacity from an oxidising to a reducing environment decreased the conductivity by several orders in magnitude, due to the reduction of Fe^{3+} to Fe^{2+}. This result clearly exhibited the importance of oxygen fugacity control in the experiments. If, e.g., the chemical composition is fixed to that of a typical mantle-olivine with 8–12% fayalite content, then the actual experimental temperature defines the number and mobility of the charge carriers,

while the variation of oxygen fugacity from reducing to more oxidising conditions determines the number of additional charge carriers being produced due to oxidation of Fe^{2+} into Fe^{3+} (Duba and Nicholls, 1973; Cemic et al., 1980; Duba and von der Gönna, 1994) (Figures 21 and 22).

A more detailed picture of the electrical charge transport was achieved by measuring the frequency dependence of the conductivity of Dreiser Weiher olivines and synthetic forsterite and fayalite (Manko, 1984). By measuring the complex conductivity in the frequency range 1 Hz up to 100 kHz Manko (1984) showed that the influence of grain boundary effects on the electrical conductivity is negligible at temperatures above 800 °C, whereas at frequencies below 100 Hz electrode polarisations significantly influence the transfer resistance (electrode – sample) and thus the measured conductivity. The measured frequency dispersion on forsterite powder samples could be modelled using a simple RC parallel circuit. The polarisations are due to the charge transport which is most likely a hopping mechanism of ionic voids. By way of contrast, fayalite exhibits no frequency dispersion in the frequency range 100 Hz up to 20 kHz and temperatures of up to 1200 °C. The conduction mechanism is based on the movement of electrons and defect-electrons, a finding that corresponds well with the pO_2 dependence of the conductivity. The pO_2 dependence favours a model where additional oxygen in the structure causes Fe-vacancies and Fe^{3+} ions on lattice positions. Thus the extrinsic conductivity of defect-electrons is most probable.

Schock et al. (1989) measured the conductivity and the thermoelectric Seebeck effect on olivine and synthetic forsterite to derive details of the (electronic, ionic) charge transport in the temperature range 1000 to 1500 °C and oxygen partial pressures ranging from 10^{-10} to 10^{4} Pa. In olivine they found a mixed ionic and extrinsic electronic conduction and charge transport by polarons,[1] with $Fe_{Mg}^{\bullet}$ hopping between Fe^{2+} and Fe^{3+}. At low temperatures electron holes dominate; at higher temperatures (above 1390 °C) Mg vacancies are the dominant charge carriers. Iron-free forsterite exhibited electronic conduction in the crystallographic [1 0 0] and [0 1 0] directions and movement of Mg-vacancies in the [0 0 1] direction. In the [0 0 1] direction the conductivity was higher than in the crystallographic a- and b-directions which is explained by structural arguments that favour charge transport through a less dense packed trigonal arrangement of oxygens

[1] A polaron results when an electron in the conduction band of a crystalline insulator or semiconductor polarises or otherwise deforms the lattice in its vicinity. The polaron comprises the electron plus its surrounding lattice deformation. If the deformation extends over many lattice sites, the polaron is large, and can be treated as a continuum. Charge carriers inducing strongly localised lattice distortions form small polarons (McGraw Hill, Encyclopaedia of Science and Technology).

forming one of the eight octahedral (1 1 1) planes. A pO_2 dependence was not detected.

Wanamaker and Duba (1993) published similar work on the directional dependence of charge transport in San Carlos single crystal olivine. The measurements were performed under various oxygen fugacities ranging from 10^{-6} to $10^{+0.5}$ Pa as well as under self- and pyroxene-buffered conditions. An irreversible loss of iron was detected by microprobe analysis when oxygen fugacities were adjusted to be more reducing than the wüstite–magnetite buffer. The chemistry of the system was changed due to the movement and loss of iron to the electrodes.

A more sophisticated conduction model for olivine was proposed by Constable and Roberts (1997) to explain measured thermo-power and conductivity data. If only small polarons $Fe_{Mg}^{\bullet}$ were the dominant charge carrier in the temperature range 1000–1200 °C, the thermo-powers should be higher than measured. To explain this discrepancy they introduced a constant polaron – Mg-vacancy V''_{Mg} term to fit the measured data. At temperatures below 1300 °C they assumed that charge transport is accomplished by polarons, while at temperatures above this the movement of Mg vacancies dominated. At low pO_2 conditions the contribution of V''_{Mg} is more important than that of $Fe_{Mg}^{\bullet}$, but with increasing temperature the contribution of V''_{Mg} to the total conductivity increases too. At a temperature of about 1300 °C the contributions of V''_{Mg} and $Fe_{Mg}^{\bullet}$ are about equal; this is supported by the observed change in activation energy at this temperature.

Qualitative defect models have been formulated by Hirsch and Shankland (1993) resulting in an 'effective charge carrier' model. This is based on a set of reliable defect reactions and thermodynamic data to produce an internally consistent model of defect populations. The charge transport in olivine is due to polaron dominated conduction, but with Mg-vacancies and electron mobilities being considered too. On the other hand, Duba and Constable (1993) argued that this mixed electron/polaron conduction model does not fit the electrical conductivity data or the oxygen fugacity dependence, especially for pyroxene-buffered olivines.

4.3.2. *Conductivity jumps associated with phase transitions*

4.3.2.1. *Germanate*. Due to the experimental limitations and problems already mentioned, much work has been performed on germanium olivine, a structural homologue of silicate-olivine (Yagi and Akimoto, 1974, Nover et al., 1992). The germanate phase transforms from the orthorhombic olivine into the cubic spinel-phase at much lower pressures due to the ionic radius of Ge being larger than that of Si. The transformation pressures required are in the range of 2–3 GPa instead of 12–16 GPa for silicate olivine. The control of

the experimental parameters, e.g., temperature, pressure, oxygen fugacity, was also much easier.

The conductivity jump produced by the α–β transition was measured on Mn_2GeO_4 by Yagi and Akimoto (1974). They found a discontinuous increase in conductivity by about half an order of magnitude.

Nover et al. (1992) and von der Gönna (1997) measured the conductivity change associated with the $\alpha \rightarrow \gamma$ transition on Mg-germanate using frequency dependent conductivity data. Measurements were performed in the temperature range of 845 up to 1400 °C. Oxygen fugacities varied from 10^{-9} to 10^{-4} Pa, while the activation energies were 1.05 eV for the olivine structure and 2.78 eV for the spinel structure. The change in conductivity produced by the phase transition depends on pressure; it was about half an order of magnitude at low-pressure conditions, and at higher pressures the conductivity jump was one order of magnitude. Due to nucleation of the new phase when the phase boundary was crossed from either side, long reaction times were required to reach stationary conditions. These times ranged from some hours at high temperatures up to several days at low temperatures.

4.3.2.2. *Silicate*. The first experimental results on the conductivity jump produced by the olivine-spinel phase transition were published by Akimoto (1965) on synthetic fayalite. Measurements were performed from 300 to 1200 K at pressures of 3.1 and 5.9 GPa. They measured a conductivity jump associate with the olivine-spinel transition of more than two orders of magnitude. The activation energies were found to be different for the two pressures – 0.51 eV for 3.1 GPa and 0.48 eV for 59.5 GPa. In the spinel phase the activation energies were about 0.3 eV. An experimental setup without the control of thermodynamic parameters impeded the reproducibility of data. Pressure and temperature were well defined in the conductivity measurements but oxygen fugacity was not controlled, with the consequence that it was not clear whether the data reflected the conductivity jump or simply an enhanced conductivity due to oxidation.

An increase in electrical conductivity of about one order of magnitude was reported by Omura (1991) when olivine transformed to spinel. Due to non-equilibrium problems and the oxidation state of the sample during the measurements, the result was not trusted by Duba and von der Gönna (1994). They could prove that the conductivity change is much too high due to the presence of highly conducting magnesiowüstite, a phase that forms beyond the boundary of the oxidation end of the stability field of olivine. Thus these data do not reflect the conductivity change produced by the olivine–spinel transition.

The electrical conductivity of natural olivine at high pressure was measured by Xu et al. (1998) on the polymorphs wadsleyite and ringwoodite under upper mantle conditions. Temperatures were varied from 800 to

1400 °C. The initial material was the San Carlos Olivine. They reported a conductivity jump for the transition olivine–wadsleyite of the order of 100. Charge transport was provided either by Fe^{3+} polarons or by shorter hopping distances in wadsleyite, due to the closer packing of the crystal structure. They used these data for upscaling the laboratory data by comparing them with a conductivity depth profile. The conductivity increase due to the olivine–wadsleyite transformation should be about two orders in magnitude. Due to the small change in conductivity for the transition wadsleyite–ringwoodite they suggested a conductivity change associated with the 670 km discontinuity of less than half an order of magnitude (Figure 20).

Xu et al. (2000) measured the effect of pressure at 4, 7 and 10 GPa on the conductivity of olivine at temperatures ranging from 950 to 1400 °C. Their findings confirmed the previously reported results on the role of small Fe^{3+} polarons for charge carrier transport. The relevant parameters for olivine conductivity are close to those measured at normal pressure conditions. Due to the uncertainties of oxygen fugacity conditions in the depth interval of 200–400 km, the temperatures calculated from the conductivity data may vary by 100–200 °C for a fugacity variation of four orders of magnitude.

On synthetic upper mantle rocks and natural gabbros from Oman, Bagdassarov et al. (2002) measured by means of impedance spectroscopy (frequency range from 0.01 up to 100 kHz) conductivities at pressures of 0.3, 0.5 and 1 GPa and temperatures from 790 to 1240 °C. At sub-solidus temperatures the conductivities strictly follow an Arrhenius behaviour with an activation energy of 1.15 eV, which is slightly lower than that reported by Schilling et al. (1997). The conductivity in the solid phase is about one order of magnitude higher, while the activation energy is less than that reported by Xu et al. (2000) for an identical sample (1.4 eV). This difference is explained by different settings for the oxygen fugacity in the experiments. Approaching the liquidus increases the conductivity by about 0.5 to 1.5 orders of magnitude (0.4–0.05 S/m). Stationary conditions were reached after 3 days of equilibration time. A significant pressure dependence of the conductivity was not detected.

4.3.3. *Effect of dissolved water on electrical conductivity*

Recent laboratory work (Xu et al., 2000) has demonstrated that the electrical conductivity profile of the mantle can be approximated using conductivity data of the major mantle mineral constituents. At transition zone depths the approximation shows less good agreement, indicating the lack of knowledge of the influence of minor constituents or water on the electrical conductivity of the nominally anhydrous phases. Knowing the effect of dissolved water on the electrical conductivity would thus provide some constraints on the amount of water in the transition zone.

Besides its influence on the electrical conductivity, water strongly affects the mantle's rheology and melting temperatures. Thus it is of importance for models of the thickness of the transition zone of the 410-km discontinuity. Experimental HPHT data showed that the boundary between olivine and wadsleyite tends to be sharper in hydrous peridotite systems, an effect that is based on the partitioning of water and the high diffusivity of hydrogen. This would cause a hydrous two-phase system of olivine and wadsleyite, initially extending over a depth range of 20 km, to decrease to a boundary of 5 km by gravitational equilibrium and rapid diffusion of hydrogen (Smyth and Frost, 2001, 2002). The presence of hydrogen via its mobility, influences the texture of olivine and wadsleyite in the transition zone, and thereby influences the electrical conductivity.

The recent electrical conductivity measurements of Poe et al. (2001) were performed on water-bearing wadsleyite and mixtures of San Carlos olivine, brucite and quartz at pressures of up to 12 GPa and temperatures ranging from roughly 400–1200 °C. Complex impedance data covered the frequency range from 0.1 Hz to 500 kHz, and sample conductivities were interpreted using RC parallel elements. By means of SIMS analysis (secondary ion mass spectroscopy) performed before and after the conductivity measurements, a loss of water was detected for the two samples (1.01 and 1.75% water by weight decreased down to 0.49 and 0.4% water by weight, respectively). Nevertheless the results suggest that the electrical conductivity of anhydrous wadsleyite is lower than that reported by Xu et al. (2001). A replication of the experiment revealed a water content of 0.16% by weight, and thus the Xu et al. (2001) results do not reflect anhydrous conductivity data, as reported. A hydrous pyrolytic mantle at the transition zone depth seems to be unlikely, because dry wadsleyite conductivities are in better agreement with the geophysical profiles of the mantle.

Gaillard (2001, 2003) reports on electrical conductivity measurements on silicate melts in the presence of water. The temperature dependence of the conductivity fits an Arrhenius law for both hydrous and dry obsidian, suggesting that a similar transport process operates in both melt and glass. The activation energies decreased with increasing water content (dry: 70 kJ/mol, and 1(3)% water by weight: 65(61) kJ/mol). Tracer diffusion experiments and electrical conductivity revealed that sodium is the dominant charge carrier in hydrous and dry obsidian. Thus the increase in conductivity with increasing water content reflects the higher mobility of sodium. During the melting of rocks, water is largely partitioned into the liquid together with alkali elements like sodium. Gaillard concludes that the mobility and concentration of sodium control the electrical conductivity of most terrestrical silicate melts. This was shown by conductivity measurements of hydrous rhyolite (2–3 wt % water) and anhydrous basalt that exhibited a conductivity about one order of magnitude lower than that of the rhyolite.

As the amount of water in mantle minerals is important for mantle rheology and melting, Gaillard et al. (2003) suggest the use of electrical conductivity data to estimate the mantle water content. The idea is based on the interpretation of conductivity variations of hydrous olivines that are measured under *in-situ* mantle p,T conditions. Hydrogen, the mobile form of water, would increase or decrease the conductivities as a function of concentration. To obtain more reliable laboratory mantle conductivity data they plan to consider both hydrogen concentration and self diffusion, a parameter that was ignored in previous studies. This would require the use of a modified version of the Nernst–Einstein equation relating the conductivity of dry olivine $\sigma^{\mathrm{ol}}_{\mathrm{dry}}$, the self-diffusion coefficient D_{H} and the concentration [H] of hydrogen in olivine:

$$\sigma = \sigma^{\mathrm{ol}}_{\mathrm{dry}} + D_{\mathrm{H}}[H] \tag{27}$$

4.4. Partial melts

Partial melts are one way to explain the abnormally high-electrical conductivities in lower crustal or upper mantle regions. In volcanic areas partial melts may cause lateral or vertical conductivity anomalies depending on the size and form of the magma chamber and the feeder dykes. Enhanced electrical conductivity along grain boundaries or fractures in the presence of partial melts requires an interconnected network of pathway for the molten phase. Partial melting will be observed when the solidus line in a phase diagram is crossed. This process depends on pressure, temperature, chemical composition and moisture content of the partial melting mineral phase.

Shankland and Waff (1977) interpreted abnormally high-electrical conductivities in the upper mantle as the result of partial melting. The melt fraction required to enhance the bulk conductivity up to >0.1 S/m was calculated using the effective medium theory (Shankland and Waff, 1974). The equation is functionally equivalent to the upper bound formula of Hashin and Shtrikman (1962, termed HS). The average DC conductivity σ in the HS^+ and HS^- model is defined as:

$$\begin{aligned} \sigma_{\mathrm{HS}^+} &= \sigma_{||}[(3\mathrm{x}_{|}\delta\sigma)/(3\sigma_{||} + (1 - x_{|})\delta\sigma)] \\ \sigma_{\mathrm{HS}^-} &= \sigma_{|}[3(1 - x_{|})\delta\sigma/(3\sigma_{|} - x_{|}\delta\sigma)] \end{aligned} \tag{28}$$

with $\delta\sigma = (\sigma_{|} - \sigma_{||})$ being the conductivity difference of the melt and the solid phases, respectively, and $x_{|}$ being the volume fraction of the melt. For HS^+ the melt forms a well-interconnected three-dimensional network, while HS^- consists of melt in isolated pockets. It was assued that the melt fraction forms

an interconnected network along the grain boundaries of an olivine-dominated matrix. Shankland and Waff (1977) reported a conductivity jump of about two orders of magnitude when an interconnected network was formed. Inversion of this formula allowed the melt fraction to be calculated at any given temperature for a given conductivity:

$$f = 3\sigma_m(\sigma^* - \sigma_s(/(\sigma^* + 2\sigma_m)(\sigma_m - \sigma_s) \tag{29}$$

where f is the melt fraction, σ_m and σ_s are melt and solid conductivities, and σ^* is the effective conductivity at a given temperature. Melt conductivities show only little variations (< 0.5 orders of magnitude) over a wide range of composition, and are totally independent of oxygen fugacity (Shankland, 1979). The resulting activation energy for the melt phase was of the order of about 1.1 eV. They assumed (from laboratory data) that a temperature of about 1350–1400 °C could be expected at a depth of 100 km for a measured conductivity of 0.2–0.4 S/m. Petrological restrictions concerning water content and unknown activation volume for σ_m limit the validity of this finding. Further limitations are due to the grain size of the powder samples that control the pockets in which melt may be formed. Furthermore the alkali content of the melt fraction determines the viscosity of the melt (Shankland et al., 1981).

Below the Western Cordillera in northern Chile, a pronounced high-conductivity zone (HCZ) was detected by Schilling et al. (1997). This was explained by partial melting considering the high heat flow values, < 100 mW/m^2, that were measured in that area. Impedance dispersion measurements were performed on representative samples in the frequency range 0.1 up to 10^6 Hz to prove that partial melting can increase the conductivity. Experiments were performed under controlled oxygen fugacity at temperatures up to the melting temperature of the crystalline pyroxene granulites. Oxygen fugacities were set to be in the stability field of hematite, wüstite and magnetite. At a temperature of 900 °C at sub-solidus conditions, conductivities of 2.5 mS/m were measured. The activation energy was calculated to be 1.34 eV. Above solidus temperatures the conductivity increased by more than two orders of magnitude up to 7 S/m at 1250 °C; the activation energy decreased to 1 eV. To explain the observations the modified brick layer model was used. The conductivity was calculated at a given temperature in view of the degree of interconnection of a melt fraction. It was assumed that between 14 and 27% by volume of melt fraction are required to explain the observed HCZ. The modified brick layer model is equivalent to the upper bound formula; its underlying principles were first published by Maxwell (1892).

Jegen and Edwards (1998) calculated the effective conductivities σ_{eff} of a mixture of partial melt σ_m and solid rock conductivities σ_s using the Hashin–Shtrikman and the Archie model to explain the conductivity anomaly of a

segment of the Juan de Fuca mid-ocean ridge. They assumed a conductivity contrast of 1/1000 in their calculations for this two-phase material. Melt conductivities were taken from Tyburczy and Waff (1983), ranging from 1 up to 10 S/m and temperatures ranging from 1500 to 1700 K. Three models were used in the calculations. In the first model electrical current flow within

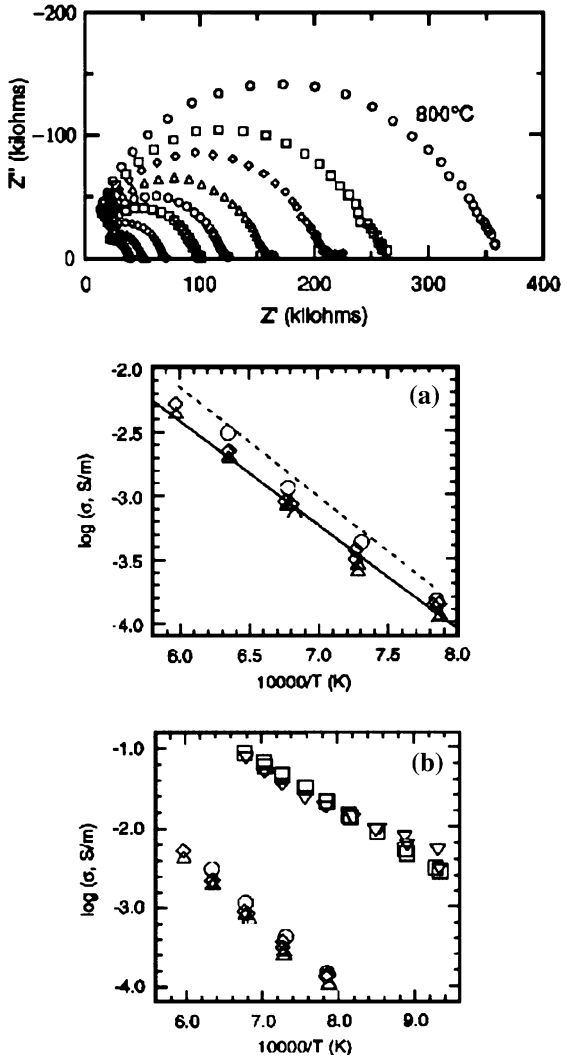

Figure 23. From top to bottom are shown: Impedance spectra of wadsleyite at 15 GPa and 800–1200 °C obtained at 50° increments. Electrical conductivity of olivine as a function of reciprocal temperature; circles, diamonds and triangles denote a olivine sample at 4, 7 and 10 GPa, respectively. Electrical conductivity of olivine, wadsleyite and ringwoodite as a function of reciprocal temperature; circles, diamonds and triangles are the same as in (b), and inverted triangles denote wadsleyite at 15 GPa, and squares denote ringwoodite at 20 GPa (Xu et al., 1998).

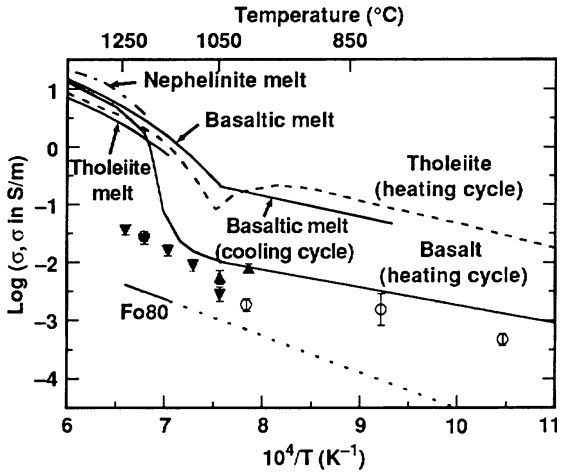

Figure 24. Log of bulk electrical conductivity vs. reciprocal temperature diagram, showing the high-frequency mechanism conductivities for the partial melts. Open and solid symbols for different experimental runs, open during the heating cycle, solid (▲) heating cycle and (▼) cooling cycle. Solid line (olivine) from Hisch et al., (1993); basalt from Presnall et al., (1972), tholeiite and nephelinite from Rai and Manghnani (1977), and tholeiite melts from Tyburczy and Waff, 1983 (Roberts and Tyburczy, 1999).

and perpendicular to the highly conducting layers was assumed. This model resulted in the lowest and highest values for melt fraction required (differing by two orders of magnitude) to obtain a high conductivity. The melt fraction required for parallel orientation was in the range 10^{-4} and 10^{-2} for perpendicular orientation. The second model was based on the lower and upper Hashin-Shtrikman bounds, resulting in an intermediate behaviour with a difference of about one order of magnitude for the melt fraction and a given effective conductivity. Aspect ratios were varied considering a variation in α ranging from 0.001 to 0.1. The final model, the Archie model, represents an average behaviour. Corresponding melt fractions of 0.14 and 0.03 for the Archie and upper HS bounds, respectively, were required to explain upper crustal conductivities.

The influence of melt composition on the electrical conductivity was studied by Roberts and Tyburczy (1999) for olivine + 5% by weight powdered basalt, and a tholeiitic mid-ocean ridge basalt (MORB) from the Juan de Fuca Ridge (Figure 23, 24). A significant variation of the electrical properties depending on temperature, melt fraction and melt composition was detected (0% at 1100 °C; 14% at 1400 °C). Above the solidus > 1120 °C, melt forms and increases the conductivity. Due to equilibrium reactions between the solid phase and melt, the melt composition changes significantly up to 1244 °C (decrease of potassium, sodium and silicon oxide and an increase of FeO). Assuming that the proportion of melt in interconnected tubes and isolated

pockets does not change, the melt conductivity is more or less constant. The parallel HS upper bound and the Archie model are both well suited to describe the measured increase in conductivity that was more by than one order of magnitude.

Partzsch et al. (2000) and Schilling and Partzsch (2001) measured the complex electrical impedance of fine grained, quartz free granulite in the frequency range from 0.1 up to 100 kHz at temperatures between 600 and 1200 °C. The sample composition was representative of lower crustal rocks. At temperatures <1030 °C a linear temperature dependence of the conductivity following an Arrhenius like behaviour was observed. The activation energy was calculated to be 1.4 eV. Above this threshold temperature the conductivity increased by more than 1.5 orders of magnitude up to a temperature of 1100 °C. The slope of the curve flattened at temperatures >1100 °C. Partial melting started above 1030 °C. This was confirmed independently by thin section analysis of the recovered samples, and by an interpretation of the complex electrical response. A melt fraction of 2% was detected at a temperature of 1040 °C, mainly concentrated in melt pockets, with a small portion of already coated grains which did not form an interconnected network. At a temperature of about 1070 °C, approximately 8% by volume of the sample is molten and forms an interconnected film along grain boundaries. Modelling of the data was done using the modified brick layer model (MBLM) assuming a melt of a conductivity of 10 S/m and an activation energy of 1 eV. The solid mineral phases had a conductivity of about 0.01 S/m and an activation energy of 1.4 eV. To produce the observed conductivity anomaly beneath the Andes Orogen, a melt fraction of 14 up to 27% by volume of interconnected melt was required. For the Pyrenees and the Tibetian Plateau from 4 to 12% by volume melt fraction was required to explain the observed conductivity. The upper bound HS model was used for the calculations (Figure 24).

Scarlato et al. (2001) measured the electrical conductivity of basaltic rocks from Mt. Etna, Sicily, at sub-solidus conditions in the temperature range of 400 to 900 °C and at frequencies from 0.1 to 100 kHz. No pressure dependence of the conductivity was detected, while the temperature dependence showed an Arrhenius like behaviour with an activation energy of less than 1 eV. Melt experiments indicated that the conductivity depends on the melt fraction, if sufficiently high, and the conductivity increased by about a factor of five.

Similar results obtained by Nover et al. (2004a, 2004b, 2006) who measured basalt and tuff from Reunion Island. The electrical data were measured in the frequency range from 1 up to 100 kHz on samples exposed to pressures corresponding to 2 km in depth. The complex data were subsequently interpreted by fitting RC model data to the measurements, at temperatures ranging from 500 to 1400 °C. Below the solidus temperature an Arrhenius behaviour of the conductivity was detected when the activation energy was 0.95 eV. Up to a

temperature of approximately 800 °C recrystallisation took place, while at temperatures above 900 °C the conductivity was increased due to the charge transport in the partial melt. Above the solidus the conductivity was increased by about 1.5 orders of magnitude when the melt fraction was sufficiently high. In terms of dielectric properties the formation of partial melt means that the dielectric constant should be enhanced. Parallel with the electrical data crystallographic structural data were obtained using the synchrotron source (DESY, Hamburg), with energy dispersive X-ray diffraction techniques in a multi-anvil high-pressure cell. Pressures and temperatures were identical to those of the conductivity measurements. The formation of a melt phase was detected as an increase of the background intensity in the diffraction diagrams at temperatures above 900 °C, up to 1350 °C. Above 1350 °C the melt fraction approaches 100% by volume; this correlates with the electrical data that indicated the existence of a fluid phase in the same temperature interval.

5. Conclusions

Some main conclusions of this paper may be summarised as follows:

(1) *Electrolytic conduction:*

- The rock fabric causes anisotropy of the conductivity,
- an interconnected network is required for electrolytic charge transport,
- the results of measurements of electrolytic conduction can give estimates on the transport properties of rocks,
- surface conductivity is important in tight rocks that are low in porosity and permeability,
- electrochemical fluid–solid interactions can be measured using impedance spectroscopy.

(2) *Electronic conduction:*

- Stress or tectonic movement favours graphitisation at low p,T conditions,
- transport and graphitisation of biogenic carbon (solid phase) are fairly well understood,
- the process of abionic (gas-phase) graphite precipitation and transport needs to be studied more thoroughly.

(3) *Semiconduction:*

- Figure 20 presents a most important result,
- the conductivities of olivine and peridotites must be measured under controlled thermodynamic conditions and controlled oxygen fugacity,

- semiconduction depends on extrinsic and intrinsic defect concentrations,
- the temperature dependence of the conductivity follows an Arrhenius behaviour,
- stationary (equilibrium) conditions require long reaction times to be established,
- the pressure effect on the conductivity is low, if no phase transitions occur,
- single crystals exhibit an anisotropy in regard to the crystallographic orientations x, y, z; polaron hopping dominates in the [0 0 1] direction,
- no reliable data on the olivine–spinel transformation are available.

(4) *Partial melts:*

- Partial melting starts from grain boundaries,
- fluid (water) content decreases the melting temperature,
- conductivity decreases when charge transport is possible through an interconnected film coating the grains,
- complex impedance is sensitive to partial melting prior to network formation (detects the shift due to dielectric change).

Acknowledgements

I would like to thank the editors of this special issue George Jiracek and Alan Chave, the reviewers Jeff Roberts and Gary Olhoeft and the anonymous reviewers. I would like to address special thanks to the editor Michael Rycroft. They all enhanced the scientific content of this review paper significantly with their fair comments and remarks. Michael Poelchau enhanced the readability of this paper by correcting the English spelling and discussing formal points. This review would never have been written without the invitation of Pasqual. Tarits who requested me to present an overview talk at the Santa Fe meeting in 2002.

References

Archie, G.: 1942. 'The Electrical Resistivity Log as an Aid in Determining Some Reservoir Characteristics', *Trans. Am. Inst. Mineral. Met.* **146**, 54–62.

Akimoto, S. I. and Fujisawa, H.: 1965. 'Demonstration of the Electrical Conductivity Jump Produced by the Olivine Spinel Transition', *J. Geophys. Res.* **70**, 443–449.

Bagdassarov, N., Schmeling, H., and Ildefonse, B.: 2002, 'Partial Melting of Mafic Rocks from Electrical Impedance Spectroscopy Measurements', Pers. commun.

Bauerle, I. E.: 1969. 'Study of Solid Electrolyte Polarisation by a Complex admittance Method', *J. Phys. Chem. Solids* **30**, 2657–2670.

Bernabe, Y.: 1986. 'Pore Volume and Transport Changes During Pressure Cycling of Several Crystalline Rocks', *Mech. Mater.* **5**, 235–249.

Bernabe, Y.: 1988. 'Comparison of Effective Pressure Law for Permeability and Resistivity formation Factor in Chelmsford Granite', *PAGEOPH* **127**, 607–625.

Bonijoly, M., Oberlin, M. and Oberlin, A.: 1982. 'A Possible Mechanism for Natural Graphite Formation', *Int. J. Coal Geol.* **1**, 283–313.

Börner, F.D. and Schön, J. H.: 1995. 'Low Frequency Complex Conductivity Measurements of Microcrack Properties', *Surv. Geophys.* **16**, 121–135.

Campbell, W.H.: 1987. 'Introduction to Electrical Properties of the Earth's Mantle', *PAGEOPH* **125**, 194–204.

Carman, P.C.: 1965, *Flow of Gases Through Porous Media*, Butterworth Scientific Publications, London.

Cemic, L., Hinze, E. and Will, G.: 1978. 'Messung der Elektrischen Leitfähigkeit bei Kontrollierten Sauerstoffaktivitäten in Druckapparaturen mit festen Drückübertragungsmedien', *High Temp. High Pres.* **10**, 469–472.

Cemic, L., Will, G. and Hinze, E.: 1980. 'Electrical Conductivity Measurements on Olivines Mg_2SiO_4–Fe_2SiO_4 Under Defined Thermodynamic Conditions', *Phys. Chem. Min.* **6**, 95–107.

Cole, K.S. and Cole, R.H.: 1941. 'Alternating Current Characteristics', *J. Chem. Phys.* **9**, 341–351.

Constable, S.C. and Duba, A.G.: 1990. 'Electrcal Conductivity of Olivine, a Dunite and the Mantle', *J. Geophys. Res.* **95**, 6967–6978.

Constable, S.C., Shankland, T.J. and Duba, A.G.: 1992. 'Conductivity of Isotropic Olivine', *J. Geophys. Res.* **97**, 3397–3404.

Constable, S.C. and Roberts, J.J.: 1997. 'Simultaneous Modelling of Thermopower and Electrical Conduction in Olivine', *Phys. Chem. Min.* **24**, 319–325.

Dachnov, W.N.: 1975, in: Schön, Petrophysik, Enke Verlag, Stuttgart, ISBN 3-432-92971-4.

David, C. and Darot, M.: 1989. 'Permeability and Conductivity of Sandstones', in V. Maury, D. Fourmaintroux, and V. Maury (eds.), *Proc. Symp. 'Rock at great depth'*, Rotterdam, The Netherlands, pp. 203–209.

David, C., Gueguen, Y. and Pmpoukis, G.: 1990. 'Effective Medium Theory and Network Theory Applied to the Transport Properties of Rocks', *J. Geophys. Res.* **95**, 6993–7005.

Debye, P.: 1927, *Polare Molekeln*, Verlag S. Hirzel, Leipzig.

Debye, P.: 1913. 'Zur Theorie der Anomalen Dispersion im Gebiet der Langwelligen Elektrischen Strahlung', *Ber. Der Dt. Phys. Ges.* **15**, 777–793.

Duba, A. and Nicholls, I.A.: 1973. 'The Influence of Oxidation State on the Electrical Conductivity of Olivine', *Earth Planet. Sci. Lett.* **18**, 59–64.

Duba, A., Heard, C. and Schock, R.N.: 1974. 'Electrical Conductivity at High Pressure and Under Controlled Oxygen Fugacity', *J. Geophys. Res.* **79**, 1667–1673.

Duba, A. and Shankland, T.J.: 1982. 'Free Carbon and Electrical Conductivity in the Earth's Mantle', *Geophys. Res. Lett.* **9**, 1271–1274.

Duba, A., Heikamp, S., Meurer, H.J., Nover, G. and Will, G.: 1994. 'Evidence from Borehole Samples for the Role of Accessory Minerals in Lower-Crustal-Conductivity', *Nature* **367**, 59–61.

Duba, A., Huenges, E., Nover, G., Will, G. and Jödicke, H.: 1988. 'Impedance of Blackshale from Münsterland 1 Borehole: An Anomalous Good Conductor?', *Geophys. J.* **94**, 413–419.

Duba, A. and Constable, S.: 1993. 'The Electrical Conductivity of a Lherzolite', *J. Geophys. Res.* **98**, 11885–19000.

Duba, A., Mathez, E.A., and Shankland, T.J.: 1982, 'Workshop Addresses Crustal Carbon and its Effect on Electrical Conductivity', *EOS*, **82**(40), 456.

Duba, A. and Gönna, J.von der: 1994. 'Comment on the Change of Electrical Conductivity of Olivine associated with the Olivine–Spinel Transition', *Phys. Earth Planet. Inter.* **82**, 75–77.

ELEKTB Group.: 1997. 'KTB and the Electrical Conductivity of the Crust', *J. Geophys. Res.* **102**, 18289–18305.

El-Kaliouby, H.M., Hussain, S., ElDiwany, E.A., Hashish, E., Bayoumi, A.R., and Poulton, M..M. (2001). Forward Modelling and inversion of IP Effects in TEM Response Using Measured Rock Samples Data. Pers. commun.

Fonton, S.de, Oberlin, A. and Inagaki, M.: 1980. 'Characterisation by Electron Microscopy of Carbon Phases (Intermediate Turbostratic Phase and Graphite) in Hard Carbons when Heattreated Under Pressure', *J. Mater. Sci.* **15**, 909–917.

Fowler, C.M.R., Stead, D., Pandit, B.I., Janser, B.W., Nisbet E.G., and Nover, G.: 2005, 'A Data Base of Physical Properties of Rocks from the Trans-Hudson Orogen, Canada', *Can. J. Earth Sci.* in press.

Freund, D. and Nover, G.: 1995. 'Hydrostatic Pressure Tests for the Permeability – Formation Factor Relation on Crystalline Rocks from the KTB Drilling Project', *Surv. Geophys.* **16**, 47–62.

Fuller, B.D. and Ward, S.H.: 1970. 'Linear System Description of Electrical Parameters of Rocks', *IEEE Trans.* **GE-8**(1), 7–13.

Gaillard, F.: 2001, 'Electrical Conductivity of Water-Bearing Magmas as a tool for Estimating Magmas Water Content?', Annual Report, 3.6.c, Bayrisches Geoinstitut.

Gaillard, F.: 2003, 'Laboratory Measurements of Electrical Conductivity of Hydrous and Dry Silicate Melts Under Pressure', Annual Report, 3.7.e, Bayrisches Geoinstitut.

Gaillard, F., Bromiley, F.A., Bromiley, G.D., Rubie, D.C., and Poe, B.T.: 2003, 'Mapping Water Distribution in the Earth's Mantle by Combining Geophysical and Laboratory Methods', Annual Report, 3.6.h., Bayrisches Geoinstitut.

Glover, P.W.J. and Vine, F.J.: 1992. 'Electrical Conductivity of Carbon Bearing Granulite at Raised Temperatures and Pressures', *Nature* **360**, 723–725.

Glover, P.W.J., Meredith, P.G., Sammons, P.R. and Murrell, A.F.: 1994. 'Ionic Surface Electrical Conductivity in Sandstone', *J. Geophys. Res.* **99**, 21635–21650.

Glover, P.W.J. and Vine, F.J.: 1995. 'Beyond KTB – Electrical Conductivity of the Deep Continental Crust', *Surv. Geophys.* **16**, 5–36.

Glover, P.W.J., Gomez, J.B., Meredith, P.G., Boon, S.A., Sammonds, P.R. and Murrell, S.A.F.: 1996. 'Modelling the Stress–strain Behaviour of Saturated Rocks Undergoing Triaxial Deformation Using Complex Electrical Conductivity Measurements', *Surv. Geophys.* **17**, 307–330.

Haak, V. and Hutton, V.R.S..: 1986. 'Electrical Resistivity in the Continental Lower Crust', in J.B. Dawson, D.A. Carswell, J. Hall, and K.H. Wedepol (eds.), *The Nature of the Lower Continental Crust*, 24 Spec. Pub.Geol. Soc., London, pp. 35–49.

Hashin, Z. and Shtrikman, A.: 1962. 'A Variational Approach to the Theory of Effective Magnetic Permeability of Multiphase Materials', *J. Appl. Phys.* **33**, 3125–3131.

Haslund, E. and Nost, B.: 1998. 'Determination of Porosity and formation Factor of Water Saturated Porous Specimens from Dielectric Dispersion Measurements', *Geophysics* **63**, 149–153.

Heikamp, S. and Nover, G.: 2003. 'An Integrated Study on Physical Properties of a KTB Gneiss Sample and a Marble from Portugal: Pressure Dependence of the Permeability and

Frequency Dependence of the Complex Electrical Impedance', *Pure Appl. Geophys.* **160**, 929–936.

Hinze, E., Will, G., Cemic, L., and Manko, M.: 1982, 'Electrical Conductivity Measurements on Synthetic Olivines at High Pressures and Temperatures Under Defined Thermodynamic Conditions', in: W. Schreyer (ed.), *High Pressure Research in Geoscience*, Schweizerbart'sche Verlagsbuchhandlung, Stuttgart.

Hinze, E., Will, G. and Cemic, L.: 1981. 'Electrical Conductivity Measurements on Synthetic Olivines and on Olivine, Enstatite and Diopsid from Dreiser Weiher, Eifel, Germany Under Defined thermodynamic activities as a Function of High Pressure and Temperature', *Phys. Earth Planet. Int.* **25**, 245–254.

Hirsch, L.M. and Shankland, T.J.: 1993. 'Qualitative Olivine Defect Chemical Model: insight on Electrical Conduction, Diffusion and the Role of Fe Content', *Geophys. J. Int.* **114**, 21–35.

Hirsch, L.M. and Shankland, T.J.: 1993. 'Electrical Conduction and Polaron Mobility in Fe-Bearing Olivine', *Geophys. J. Int.* **114**, 36–44.

Hoffmann, N., Jödicke, H. and Gerling, P.: 2001. 'The Distribution of Pre-Westfalian Source Rocks in the North German Basin – Evidence from Magnetotelluric and Geochemical Data', *Geologie en Mijnbouw/ Nederlands J. Geosci.* **80**(1), 71–84.

Jegen, M. and Edwards, R.N.: 1998. 'The Electrical Properties of a 2D Conductive Zone Under the Juan De Fuca Ridge', *Geophys. Res. Lett.* **25**, 3647–3650.

Jödicke, H., Kruhl, J.H., Ballhaus, C., Giese, P. and Untiedt, J.: 2004. 'Syngenetic Thin Graphite Rich Horizons in Lower Crustal Rocks from the Serr San Bruno, Calabria (Italy), and Implications for the Nature of High Conducting Deep Crustal Layers', *Phys. Earth Planet. Int.* **141**, 37–58.

Johnson, D.L. and Manning, H.J.: 1986. 'Theory of Pressure Dependent Resistivity in Crystalline Rocks', *J. Geophys. Res.* **91**, 11611–11617.

Johnson, D.L. and Sen, P.N.: 1988. 'Dependence of the Conductivity of a Porous Medium on Electrolyte Conductivity', *Phys. Rev. B* **33**, 3502–3510.

Jonscher, A.K.: 1975. 'The Interpretation of Non-ideal Admittance and Impedance Diagrams', *Phys. State Sol.* **32**, 665–676.

Jonscher, A.K.: 1978. 'Analysis of Alternating Current Properties of Ionic Conductors', *J. Mater. Sci.* **13**, 553–562.

Knight, R.J. and Nur, A.: 1987. 'The Dielectric Constant of Sandstones, 60 kHz to 4 MHz', *Geophysics* **52**, 644–654.

Knight, R.J.: 1991. 'Hysteresis in the Electrical Resistivity of Partially Saturated Sandstones', *Geophysics* **56**, 2139–2147.

Kontny, A., Friedrich, H., Behr, H.J., DeWall, H., Horn, E., Möller, P. and Zulauf, G.: 1997. 'Formation of Ore Minerals in Metamorphic Rocks of the German Continental Deep Drilling Site (KTB)', *J. Geophys. Res.* **102**, 18,323–18,336.

Losito, G., Schnegg, P.A., Lambellet, C., Viti, C. and Trova, A.: 2001. 'Microscopic Scale Conductivity as Explanation of Magnetotelluric Results from the Alps of West Switzerland', *Geophys. J. Int.* **147**, 602–609.

Manko, M.: 1984, 'Die frequenzabhängige elektrische Leitfähigkeit von Forsterit und Fayalit sowie von Olivin Peridotit Xenolithen des Dreiser Weihers unter hohen Drücken und definierten SiO2 Aktivitäten als Funktion von Temperatur und Sauerstoffugazität', PhD-Thesis, Universität Bonn.

Maumus, J., Bagdassarov N., Schmeling H., and Ildefonse B.: 2001, 'Partial Melting of Mafic Rocks from Electrical Impedance Spectroscopy Measurements', Www.geophysik.-uni-frankfurt.de/∼nickbagd/posterga.htm.

Mendelson, K.S. and Cohen, M.H.: 1982. 'The Effect of Grain Anisotropy on the Electrical Properties of Sedimentary Rocks', *Geophysics* **47**, 257–263.

Mogk, D.W., and Mathez, E.A.: 2000, 'Carbonaceous Films in Midcrustal Rocks from the KTB Borehole, Germany, as Characterised by Time-of-Flight Secondary Ion Mass Spectroscopy', *Geochem. Geophys. Geosyst.* G^3, 2000GC000081.

Monteiro Santos, F.A., Mateus, A., Almeida, E.P., Pous J., and Mendes-Victor, L.: 2002, 'Are Some of the Deep Crustal Conductive Features Found in SW Iberia Caused by Graphite?', *Earth Planet. Sci. Lett.*, 353–367.

Morat, P. and Le Mouel, J.L.: 1987. 'Variation of the Electrical Resistivity of Large Rock Samples with Stress', *Geophysics* **32**, 1424–1430.

Morat, P., and Le Mouel, J.L.: 1992, 'Electrical Signals Generated by Stress Variations in Porous Non-saturated Rocks', *C.R. Academie Science, Paris*, **315**, 955–963.

Nover, G., Will, G. and Waitz, R.: 1992. 'Pressure induced Phase Transitions in Mg_2GeO_4 as Determined by Frequency Dependent Complex Electrical Resistivity Measurements', *Phys. Chem. Min.* **19**, 133–139.

Nover, G., Heikamp, S., Kontny, A. and Duba, A.: 1995. 'The Effect of Pressure on the Electrical Conductivity of KTB Rocks', *Surv. Geophys.* **16**, 63–81.

Nover, G., Heikamp, S., Meurer, H.J. and Freund, D.: 1998. 'In situ Electrical Conductivity and Permeability of Mid-Crustal Rocks from the KTB Drilling: Consequences for High Conductive Layers in the Earth Crust', *Surv. Geophys.* **19**, 73–85.

Nover, G. and Heikamp, S.: 2000. 'Electrical Impedance Spectroscopy Used as a Tool for the Detection of Fractures in Rock Samples Exposed to Either Hydrostatic or Triaxial Pressure Conditions', *Natural Hazards* **21**, 317–330.

Nover, G. and Heikamp, S.: 2001. 'The Electrical Signature of Rock Samples Exposed to Hydrostatic and Triaxial Pressures', *Annali di Geofisika* **44**, 287–294.

Nover, G., von der Gönna, J., and Meurer, HJ.: 2004b, 'Electrical Conductivity of Reunion Island Basalt and Tuff', *Geophys. J. Int.* in preparation.

Nover, G., and Stoll, J.B.: 2005, 'Promotion of Graphite formation by Tectonic Stress – A Laboratory Experiment', *Geophys. J. Int.*, **160**, 1059–1067.

Nover, G., Heikamp, S., Dürrast, H., and Siegesmund, S.: 2005, 'Relationship Between Electrical and Hydraulic Properties of Reservoir Rocks', *Geophys. J. Int.*, accepted.

Oberlin, A.: 1984. 'Carbonisation and Graphitisation', *Carbon* **22**, 521–541.

Olhoeft, G.R..: 1976. 'Electrical Properties in Rocks', in R.J.G. Strens (ed.), *The Physics and Chemistry of Rocks and Minerals.*, Wiley, London, pp. 261–278.

Olhoeft, GR.: 1979. 'Electrical Properties. Initial Report on the Petrophysics Laboratory', *U.S. Geol. Survey Circular* **789**, 1–26.

Olhoeft, G.R.: 1985, Low Frequency Electrical Properties', *Geophysics*, **50**, 2492–2503.

Olhoeft, G.R.: 1987, 'Electrical Properties from 10.3 to 109 Hz- Physics and Chemistry in Physics and chemistry of Porous Media II', in: J.R. Bnavar, J. Koplik. and K.W. Winkler (eds.), *AIP Conference Proceedings 154*, American Institute of Physics, New York, pp. 281–298.

Omura, K.: 1991. 'Change of Electrical Conductivity of Olivine associated with the Olivine–spinel Transition', *Phys. Earth Planet. Inter.* **65**, 292–307.

Pape, H., Riepe, L., and Schopper, JR.: 1981, 'Calculating Permeability from Surface Area Measurements', in: Porceedings of the Seventh Eur. Logg. Symp. Trans., Paris.

Pape, H., Clauser, C. and Iffland, J.: 1999. 'Variation of Permeability with Porosity in Sandstone Diagenesis Interpreted with Fractal Pore Space Model', *Geophysics* **64**, 1447–1460.

Partzsch, G.M., Schilling, F.R. and Arndt, J.: 2000. 'The influence of Partial Melting on the Electrical Behaviour of Crustal Rocks: Laboratory Examinations, Model Calculations and Geological interpretations', *Tectonophysics* **317**, 189–203.

Poe, B.T., Romanero, C., and Tyburzcy, J.: 2001, 'Effect of Dissolved Water on the Electrical Conductivity of Wadsleyite', Annual Report, Bayrisches Geoinstitut.
Revil, A., Darot, M. and Pezard, P.A.: 1996. 'From Surface Electrical Properties to Spontaneous Potentials in Porous Media', *Surv. Geophys.* **17**, 331–346.
Revil, A., Cathles, L.M. III, Losh, S. and Nunn, J.A.: 1998. 'Electrical Conductivity in Shaly Sands with Geophysical applications', *J. Geophys. Res.* **103**, 23925–23936.
Roberts, J.J. and Tyburczy, J.A.: 1993. 'Frequency Dependent Electrical Properties of Dunite as Functions of Temperature and Oxygen Fugacity', *Phys. Chem. Min.* **19**, 545–561.
Roberts, J.J. and Tyburczy, J.A.: 1993. 'Impedance Spectroscopy of Single and Polycrystalline Olivine: Evidence for Grain Boundary Transport', *Phys. Chem. Min.* **20**, 19–26.
Roberts, J.J. and Tyburczy, J.A.: 1999. 'Partial Melt Electrical Conductivity: influence of Melt Composition', *J. Geophys. Res.* **104**, 7055–7065.
Roberts, J.J., Duba, A.G., Mathez, E.A., Shankland, T.J. and Kinzler, R.: 1999. 'Carbon-Enhanced Electrical Conductivity During Fracture of Rocks', *J. Geophys. Res.* **104**, 737–747.
Roberts, J.J., Ramirez, A., Carlson, S., Ralph, W., Bonner, B.P. and Daily, W.: 2001. 'Laboratory and Field Measurements of Electrical Resistivity to Determine Saturation and Detect Fractures in a Heated Rock Mass', *Geothermal Resources Council Trans.* **25**, 26–29.
Roberts, J.J.: 2002. 'Electrical Properties of Microporous Rock as a Function of Saturation and Temperature', *J. Appl. Phys.* **91**, 1687–1694.
Rouzaud, J., Oberlin, A., Deurbergue, A., and Kwak, Y.H.: 1990, 'Structural Study of Graphitisation in the Moongyeong Coalfield South Korea', Bull. Soc. Geol. Fr. Spec. Congr. Coal Formation, Occurrence and Related Properties, Orleans.
Ross, J.V. and Bustin, R.M.: 1990. 'The Role of Strain Energy in Creep Graphitisation of anthracite', *Nature* **343**, 58–60.
Ross, J.V., Bustin, R.M. and Rouzaud, J.N.: 1991. 'Graphitisation of High Rank Coals – the Role of Shear Strain: Experimental Considerations', *Organ. Geochem.* **17**, 585–596.
Ruffet, C., Gueguen, Y. and Darot, M.: 1991. 'Complex Conductivity Measurements and Fractal Nature of Porosity', *Geophysics* **56**, 758–768.
Ruffet, C., Darot, M. and Gueguen, Y.: 1995. 'Surface Conductivity in Rocks: A Review', *Surv. Geophys.* **16**, 83–105.
Scarlato, P., Freda, C., and Poe, BT.: 2001, 'HP–HT Measurements of Electrical Conductivity in Basaltic Rocks from Mt. Etna, Sicily, Italy', Annual Report, Bayrisches Geoinstitut.
Schilling, F.R. and Partzsch, G.M.: 2001. 'Quantifying Partial Melt Fraction in the Crust Beneath the Central andes and the Tibetan Plateau', *Phys. Chem. Earth* **26**, 239–246.
Schock, R.N., Duba, A.G. and Shankland, T.J.: 1989. 'Electrical Conduction in Olivine', *J. Geophys. Res.* **94**, 5829–5839.
Schön, J.: 1983, *Petrophysik*, Enke Verlag Stuttgart.
Schilling, F.R., Partzsch, G.M., Brasse, H. and Schwarz, G.: 1997. 'Partial Melting Below the Magmatic arc in the Central andes Deduced from Geoelectromagnetic Field Experiments and Laboratory Data', *Phys. Earth Planet. Int.* **103**, 17–31.
Sen, P.N.: 1981. 'Relation of Certain Geometrical Features to the Dielectric anomaly of Rocks', *Geophysics* **46**, 1714–1720.
Sen, P.N.: 1984. 'Grain Shape Effects on Dielectric and Electrical Properties of Rocks', *Geophysics* **49**, 586–587.
Shankland, T.J. and Waff, H.S.: 1974. 'Conductivity in Fluid Bearing Rocks', *J. Geophys. Res.* **79**, 4863–4868.
Shankland, T.J. and Waff, H.S.: 1977. 'Partial Melting and Electrical Conductivity Anomalies in the Upper Mantle', *J. Geophys. Res.* **82**, 5409–5417.

Shankland, T.J.: 1979. 'Physical Properties of Minerals and Melts', *Rev. Geophys. Space Phys.* **17**, 792–802.

Shankland, T.J., O'Connell, R.J. and Waff, H.S.: 1981. 'Geophysical Constraints on Partial Melt in the Upper Mantle', *Rev. Geophys. Space Phys.* **19**, 394–406.

Shankland, T.J., Duba, A.G., Mathez, E.A and Peach, C.L.: 1997. 'Increase of Electrical Conductivity with Pressure as an Indicator of Conduction Through a Solid Phase in Midcrustal Rocks', *J. Geophys. Res.* **102**, 14741–14750.

Stoll, J.: 1993. 'A Mise-a-la-masse Experiment for Detecting an Electric Network around the KTB', *KTB-Report* **93–2**, 361–364.

Stoll, J., Bigalke, J. and Grabner, E.W.: 1995. 'Electrochemical Modelling of Self Potential Anomalies', *Surv. Geophys.* **16**, 107–120.

Stoll, J., Haak, V. and Spitzer, K.: 2000. 'The Electrical Double Dipole Experiment in the KTB Deep Borehole', *J. Geophys. Res.* **105**, 21319–21331.

Teichmüller, R., and Teichmüller M.: 1982, 'Inkohlungsgradienten in der Anthrazitfolge des Ibbenbürener Karbons', *Fortschr. Geol. Rheinl. u. Westf.*, **27**, 201–276.

Tyburczy, J.A. and Waff, H.S.: 1983. 'Electrical Conductivity of Molten Basalt and Andesite to 25 Kilobars Pressure: Geophysical Significance and Implications for Charge Transport and Melt Structure', *J. Geophys. Res.* **88**, 2413–2430.

von der Gönna, J.: 1997 'In situ Untersuchungen zur Phasentransformation Olivin-Spinell im Modellsystem Mg2GeO4 mittels Impedanzspektroskopie und energiedispersiver Röntgenbeugung', PhD Thesis, University Bonn.

Vanhala, H. and Soininen, H.: 1995. 'Laboratory Technique for Measurement of Spectral induced Polarisations Response of Soil Samples', *Geophys. Prospect.* **43**, 655–676.

Vanhala, H.: 1997, 'Laboratory and Field Studies of Environmental and Exploration applications of the Spectral induced-Polarisation (SIP) Method', PhD Thesis, Geological Survey of Finland.

Waff, H.S.: 1974. 'Theoretical Considerations of Electrical Conductivity in a Partial Molten Mantle and Implications for Geothermometry', *J. Geophys. Res.* **79**, 4003–4010.

Walter, J., and Althaus, E.: 1993, 'Graphite Deposition in Tectonically Mobilised Fault Planes of the KTB Pilot Drill Hole', KTB-Report, 93-2, 455–460.

Wanamaker, B.J. and Duba, A.G.: 1993. 'Electrical Conduction of San Carlos Olivine along [001] Under Oxygen- and Pyroxene Buffered Conditions', *J. Geophys. Res.* **98**, 489–500.

Waxman, M.H., and Smits, L.J.: 1968, 'Electrical Conduction in Oil Bearing Sands', *Soc. Petr. Eng. J.*, **8**, 107–122.

Wilks, K.R., Mastalerz, M., Ross, J.V. and Bustin, R.M.: 1993. 'The Effect of Experimental Deformation on the Graphitisation of Pennsylvania Anthracite', *Int. J. Coal Geol.* **24**, 347–369.

Wildenschild, D., Roberts, J.J. and Carlberg, E.D.: 2000. 'On the Relationship Between Microstructure and Electrical and Hydraulic Properties of Sand–clay Mixtures', *Geophys. Res. Lett.* **27**, 3083–3088.

Xu, Y., Poe, B.T. and Shankland, T.J.: 1998. 'Electrical Conductivity of Olivine, Wadsleyite, and Ringwoodite Under Upper Mantle Conditions', *Science* **280**, 1415–1418.

Xu, Y., Shankland, T.J. and Duba, A.G.: 2000. 'Pressure Effect on Electrical Conductivity of Mantle Olivine', *Phys. Earth Planet. Int.* **118**, 149–161.

Xu, Y. and Shankland, T.J.: 1999. 'Electrical Conductivity of Orthopyroxen and its High Pressure Phases', *Geophys. Res. Lett.* **26**, 2645–2648.

Yagi, T. and Akimoto, S.I.: 1974. 'Electrical Conductivity Jump Produced by the α–β–γ Transformation in Mn_2GeO_4', *Phys. Earth Planet. Int.* **8**, 235–240.

Zulauf, G.: 1992. 'Late to Post Variscian Deformation Phases and Paleostresses in the KTB Pilot Research well (Bohemian Massif, Germany)', *Tectonophysics* **202**, 1–21.